Atmos. Chem. Phys., 9, 3113–3136, 2009
www.atmos-chem-phys.net/9/3113/2009/

Atmospheric Chemistry and Physics

The impact of traffic emissions on atmospheric ozone and OH: results from QUANTIFY

P. Hoor[1], J. Borken-Kleefeld[2], D. Caro[3], O. Dessens[4], O. Endresen[5], M. Gauss[6], V. Grewe[7], D. Hauglustaine[3], I. S. A. Isaksen[6], P. Jöckel[1], J. Lelieveld[1], G. Myhre[6,8], E. Meijer[9], D. Olivie[10], M. Prather[11], C. Schnadt Poberaj[12], K. P. Shine[13], J. Staehelin[12], Q. Tang[11], J. van Aardenne[14], P. van Velthoven[9], and R. Sausen[7]

[1]Max Planck Institute for Chemistry, Dept. of Atmospheric Chemistry, 55020 Mainz, Germany
[2]Transportation Studies, German Aerospace Center (DLR), Berlin, Germany
[3]Laboratoire des Sciences du Climat et de l'Environment (LSCE), CEN de Saclay, Gif-sur-Yvette, France
[4]Centre for Atmospheric Science, Dept. of Chemistry, Cambridge, UK
[5]DNV, Det Norske Veritas (DNV), Oslo, Norway
[6]Dept. of Geosciences, University of Oslo, Norway
[7]Deutsches Zentrum für Luft- und Raumfahrt, Inst. für Physik der Atmosphäre, Oberpaffenhofen, 82234 Wessling, Germany
[8]Center for International Climate and Environmental Research-Oslo (CICERO), Oslo, Norway
[9]Royal Netherlands Meteorological Institute, KNMI, De Bilt, The Netherlands
[10]Meteo France, CNRS, Toulouse, France
[11]Department of Earth System Science, University of California, Irvine, USA
[12]Institute for Atmospheric and Climate Science, Swiss Federal Institute of Technology, Zürich, Switzerland
[13]Department of Meteorology, University of Reading, UK
[14]Joint Research Center, JRC, Ispra, Italy

Received: 9 July 2008 – Published in Atmos. Chem. Phys. Discuss.: 21 October 2008
Revised: 5 May 2009 – Accepted: 5 May 2009 – Published: 14 May 2009

Abstract. To estimate the impact of emissions by road, aircraft and ship traffic on ozone and OH in the present-day atmosphere six different atmospheric chemistry models have been used. Based on newly developed global emission inventories for road, ship and aircraft emission data sets each model performed sensitivity simulations reducing the emissions of each transport sector by 5%.

The model results indicate that on global annual average lower tropospheric ozone responds most sensitive to ship emissions (50.6%±10.9% of the total traffic induced perturbation), followed by road (36.7%±9.3%) and aircraft exhausts (12.7%±2.9%), respectively. In the northern upper troposphere between 200–300 hPa at 30–60° N the maximum impact from road and ship are 93% and 73% of the maximum effect of aircraft, respectively. The latter is 0.185 ppbv for ozone (for the 5% case) or 3.69 ppbv when scaling to 100%. On the global average the impact of road even dominates in the UTLS-region. The sensitivity of ozone formation per NO_x molecule emitted is highest for aircraft exhausts.

The local maximum effect of the summed traffic emissions on the ozone column predicted by the models is 0.2 DU and occurs over the northern subtropical Atlantic extending to central Europe. Below 800 hPa both ozone and OH respond most sensitively to ship emissions in the marine lower troposphere over the Atlantic. Based on the 5% perturbation the effect on ozone can exceed 0.6% close to the marine surface (global zonal mean) which is 80% of the total traffic induced ozone perturbation. In the southern hemisphere ship emissions contribute relatively strongly to the total ozone perturbation by 60%–80% throughout the year.

Methane lifetime changes against OH are affected strongest by ship emissions up to 0.21 (± 0.05)%, followed by road (0.08 (±0.01)%) and air traffic (0.05 (± 0.02)%). Based on the full scale ozone and methane perturbations positive radiative forcings were calculated for road emissions (7.3±6.2 mWm^{-2}) and for aviation (2.9±2.3 mWm^{-2}). Ship induced methane lifetime changes dominate over the ozone forcing and therefore lead to a net negative forcing (−25.5±13.2 mWm^{-2}).

Correspondence to: P. Hoor
(peter.hoor@mpic.de)

Published by Copernicus Publications on behalf of the European Geosciences Union.

1 Introduction

The rise in energy consumption by the growing human population and the increasing mobility are associated with emissions of air pollutants in particular by road and air traffic as well as international shipping. These emissions are expected to increase in future, affecting air quality and climate (Kahn Ribeiro et al., 2007) which in turn affects air pollution levels (Hedegaard et al., 2008). The impact of air traffic emissions has been subject of various investigations (e.g. Hidalgo and Crutzen, 1977; Schumann, 1997; Brasseur et al., 1996; Schumann et al., 2000) also assessing projections for the future (e.g. Sovde et al., 2007; Grewe et al., 2007). For the present day atmosphere these studies indicated an increase of ozone of 3–6% due to aircraft emissions in the region of the North Atlantic flight corridor. More recent studies calculated an overall maximum effect of 5% for the year 2000 in the northern tropopause region (Grewe et al., 2002). Depending on season the values typically range between 3 ppbv and 7.7 ppbv in January and September, respectively (Gauss et al., 2006). The global annual averaged radiative forcing due to the additional O_3 from air traffic is estimated to be of the order of 20 mW/m^2 (Sausen et al., 2005).

Relatively few studies have dealt with the impact of road traffic (Granier and Brasseur, 2003; Niemeier et al., 2006; Matthes et al., 2007), and ship emissions (Lawrence and Crutzen, 1999; Corbett and Koehler, 2003; Eyring et al., 2005; Dalsoren and Isaksen, 2006; Endresen et al., 2007; Eyring et al., 2007). Endresen et al. (2003) reported peak ozone perturbations of 12 ppbv for the marine boundary layer during northern summer over the northern Atlantic and Pacific regions. Eyring et al. (2007) used a multi-model approach based on EDGAR emissions and reported somewhat lower values of 5–6 ppbv for the North Atlantic. They also calculated a maximum column perturbation of 1 DU for the tropospheric ozone column associated with radiative forcings of 9.8 mW/m^2. For road emissions Matthes et al. (2007) found maximum contributions to surface ozone peaking at 12% in northern midlatitudes during July. Similar values of 10% are reported by Niemeier et al. (2006) for current conditions.

Besides the effects of pollutants on ozone a potential change of the OH concentration is of importance in particular for regional air quality and the self-cleaning capacity of the atmosphere (Lelieveld et al., 2002). Changes of methane loss rates due to anthropogenic emissions are reported to be on the order of 0.5%/yr of which 1/3 (0.16%) is due to an increase of OH from anthropogenic CO, NO_x and non-methane hydrocarbons (NMHCs) (Dalsoren and Isaksen, 2006). In addition, the regional OH distribution can be differ substantially due to the short lifetime of OH and NO_x in particular in the lower troposphere and the different response of the HO_x-NO_x-O_3-system to NO_x perturbations (Lelieveld et al., 2002, 2004). Although generally the presence of carbon compounds such as CH_4, NMHCs, and CO act as a sink for OH, the latter can be efficiently recycled in the presence of NO_x. The reaction of NO with HO_2 produces O_3 and recycles OH making the system less sensitive to perturbations. Pristine regions with low NO_x and high OH concentrations conditions are favourable for OH-formation following ozone production from NO_x-perturbations. Since emissions from the three transport sectors are emitted into rather different environments their impact on O_3 and OH may differ strongly.

The EU-project QUANTIFY (Quantifying the Climate Impact of Global and European Transport Systems) is the first attempt to provide an integrated and consistent view on the effects of traffic on various aspects of the atmosphere. Fuglestvedt et al. (2008) calculated that transport accounts for 31% of the man made ozone forcing since preindustrial times. Here we present simulations obtained with six different models all using the same set of emissions to provide a credible evaluation of the present-day atmospheric effects by traffic and to estimate the uncertainties of model results. This study focuses on the global impact of traffic exhaust emissions on the current chemical state of the atmosphere. The climatological implications and future projections are subject of followup studies.

2 Emissions and simulation setup

Emissions for the three transport sectors road, shipping and air traffic were replaced in the EDGAR data base with respect to the individual emission classes and recalculated separately for QUANTIFY. Emissions from road transportation were developed bottom-up: Vehicle mileage and fleet average emission factors were estimated for the year 2000. The inventory differentiates between five vehicle categories and four fuel types and covers 12 world regions and 172 countries. It is adjusted for the year 2000 to the national road fuel consumption (Borken et al., 2007, and references therein) or national statistics or own calculations. National emissions are allocated to a $1^\circ \times 1^\circ$-grid essentially according to population density with emissions from motorised two- and three-wheelers biased towards agglomerations and emissions from heavy duty vehicles biased towards rural areas. The emissions used in this study are based on a draft version (Borken and Steller, 2006). The final inventory for road traffic includes improved emission factors. With fuel consumption and CO_2 emissions only 3% higher, the final global traffic emissions of NO_x, NMHC and CO are higher by 33%, 48% and 51%, respectively. The integrated annual emissions which were used in this study for selected species had to use the draft emissions and are given in Table 1.

The emissions for ship traffic were reconstructed for QUANTIFY based on fuel- and activity-based esimates by Endresen et al. (2007). They report a fuel consumption being about 50–80 Mt ($\approx$ 70–80%) lower than in Eyring et al. (2005) or Corbett and Koehler (2003). They attribute the difference to the different assumptions for the operation at sea.

Table 1. Emissions from different sources provided by QUANTIFY for the year 2000 in TgN NO_x and TgC CO and NMHC, respectively (for NMHCs the conversion of 161/210 according to TAR was used). Soil and biogenic isoprene emissions were taken from Ganzeveld et al. (2006); Kerkweg et al. (2006), biogenic emissions of hydrocarbons and CO according to von Kuhlmann et al. (2003a,b).

	QUANTIFY[abc]			ACCENT[d]			EDGAR[ef]			RETRO[g]	
source	NO_x	CO	NMHC	NO_x	CO	NMHC	NO_x	CO	NMHC	NO_x	CO
ROAD	6.85	31.3	7.7	–	–	–	8.67	79.8	25.9	9.7[h]	91.6[h]
SHIP	4.39	0.6	0.34	–	–	–	6.3	0.55	1.3	3.6	0.47
AIR	0.67	–	–	0.79	–	–	0.71	0.04	0.42	0.73	–
tot. traffic	11.91	31.9	8.04	16.07	83.36	36.6	17.6[i]	86.6[i]	29.84[i]	–	–
Non-traffic	27.1[e]	341.3[e]	100.3[e]	21.9	447.4	76.13	27.1	341.3	100.3	19.3	275.6
biogenic, soil	6.89[j]	48.2	340.5	5	100	772	–	–	–	9.4	77.3

[a]Road emissions: Borken and Steller (2006), [b]Ship emissons: Endresen et al. (2007), [c]Aircraft emssions: Eyers et al. (2004), [d]Emission inventory developed within ACCENT (Atmospheric Climate Change: The European Network of Excellence) and GEIA (Global Emissions Inventory Activity), [e]van Aardenne et al. (2005); Olivier et al. (2005), [f]Ship emissions from Eyring et al. (2005), [g] Reanalysis of the tropospheric composition over the past 40 years, data taken from report on emissions data sets and methodologies for estimating emissions, ftp://ftp.retro.enes.org/pub/documents/reports/D1-6_final.pdf, [h]Total land based traffic, [i]Including non-road land transport, [j]Ganzeveld et al. (2006); Kerkweg et al. (2006)

For further details see Endresen et al. (2007).
Aircraft emissions are based on the AERO2K dataset (Eyers et al., 2004) including the emissions from military aviation. The emissions for each transport sector are given in Table 1.

Non-traffic emissions used in the present modelling exercise are based on the latest release of the EDGAR32FT2000 emission inventory (van Aardenne et al., 2005; Olivier et al., 2005) including emissions of greenhouse gases and ozone precursors for the year 2000 with the exception of methane. Methane was prescribed as a surface boundary condition using time dependent surface mixing ratios as in Jöckel et al. (2006) based on surface observations from the AGAGE database. For the initialization the three dimensional methane distribution from the same simulation was used.

For biomass burning monthly means for the year 2000 were used based on GFED estimates with multi-year (1997–2002) averaged activity data using Andreae and Merlet (2001) and Andreae (2004, personal communication) for NO_x emission factors (BB-AVG-AM). Lightning NO_x was specified at 5 TgN/year, representing the current best estimate (Schumann and Huntrieser, 2007).

NMHCs were subdivided into individual organic and partly oxidized species. The partitioning of the NMHCs was performed according to von Kuhlmann et al. (2003a) and is shown in Table 2 for biomass burning and fossil fuel related emissions. The mass of NMHCs given in kg(NMHC)/yr was converted to kg(C)/year using a ratio of 161/210 TgC/Tg(NMHC) for mass(Carbon)/mass(NMHC-molecule) as in the third IPCC assessment report. The specific ratios were then applied to calculate the individual NMHC partitioning.

Table 2. Fraction of individual species contributing to the total emission of NMHCs from biomass burning and fossil fuel combustion in QUANTIFY (von Kuhlmann et al., 2003a,b).

	NMHC specifications	
species	biomass burning	fossil fuel
C_2H_6	0.1014350	0.05974
C_3H_8	0.0322390	0.09460
C_4H_{10}	0.0416749	0.7154
C_2H_4	0.1904856	0.03715
C_3H_6	0.0849224	0.01570
CH_3OH	0.1075290	0.01436
CH_3CHO	0.0483586	0.
CH_3COOH	0.1136230	0.
CH_3COCH_3	0.0501278	0.02375
HCHO	0.0609397	0.004787
HCOOH	0.0404954	0.
MEK	0.1281699	0.03447

Biogenic emissions for isoprene and NO emissions from soils were also included based on online calculations with the EMAC model (ECHAM5/MESSy, atmospheric chemistry) (Ganzeveld et al., 2006; Kerkweg et al., 2006) for 1998–2005 as described in Jöckel et al. (2006). The 5-hourly output fields were converted to monthly means and provided as offline fields to all partners. Thus, seasonal cycles are represented in the biogenic fields as well as in the biomass burning emissions and the aircraft emissions, but not for ship and road traffic emissions or in the other EDGAR-based fields.

To compare the emissions provided by QUANTIFY with other projects and data bases some recently used inventories are also given in Table 1. Notably the road traffic emissions are lower than in other inventories. The final road traffic

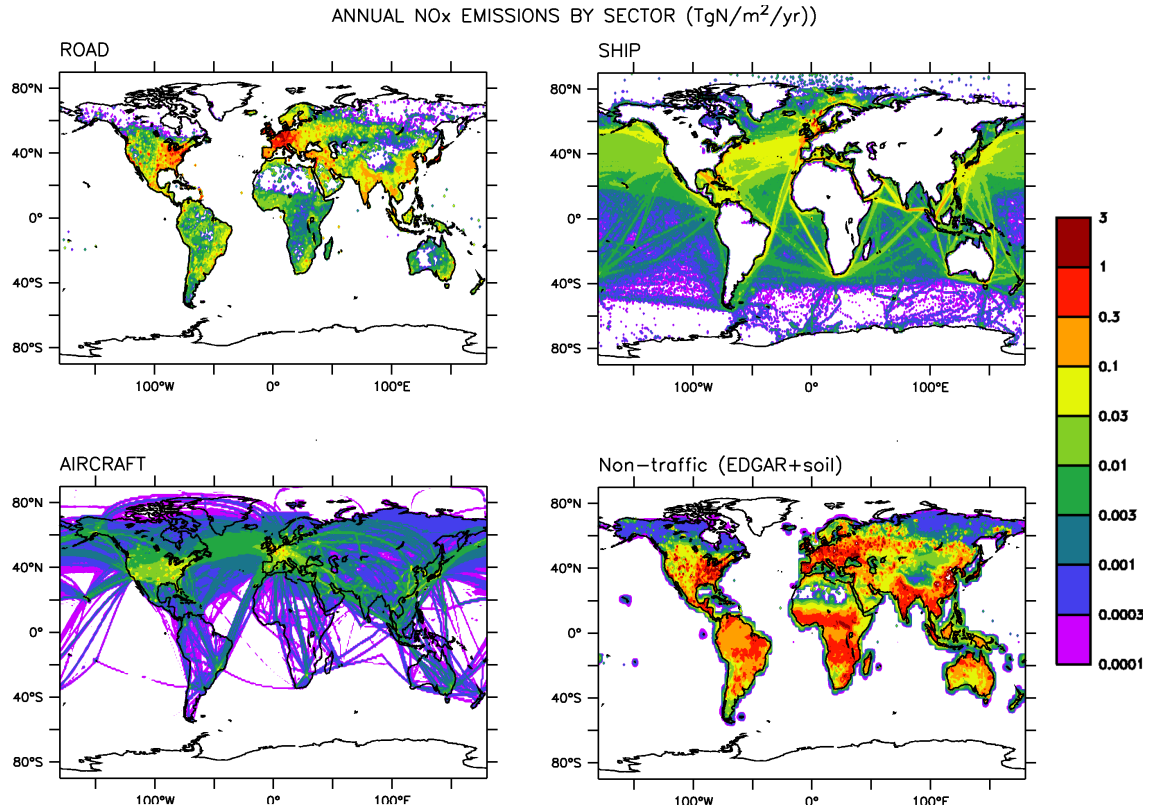

Fig. 1. NO_x emissions (TgN/m^2/year) used in QUANTIFY by sector.

Table 3. Model simulations performed for QUANTIFY.

experiment	emission		
	road	ship	aircraft
BASE	100%	100%	100%
ROAD	95%	100%	100%
SHIP	100%	95%	100%
AIR	100%	100%	95%
ALL	95%	95%	95%

emissions by Borken et al. (2007) are higher by 33% for NO_x and about 50% for CO emissions than those used in this study. Nonetheless, low total CO emissions are a result of lowered average emission factors accounting for effective use of catalytic converters in light duty vehicles.

The resulting source strengths of NO_x from the different sectors, which were used in QUANTIFY are shown in Fig. 1. Globally, road NO_x emissions are dominated by the eastern US and western Europe as well as India and eastern China, the latter with an increase rate of 6%/year (Ohara et al., 2007) only between 2000 and 2003. Besides the continental coast lines in the northern hemisphere and around the major shipping routes ship traffic over the northern central Atlantic between 25°–55° N is a significant source of NO_x over a large area. A second NO_x source from ship emissions covering a large area is traffic along the east coast of Asia. Besides the continental eastern US and western Europe the largest emissions from air traffic also occur over the North Atlantic, though further north than the shipping maxima. In the southern hemisphere NO_x emissions are largely dominated by non-traffic sources and biomass burning.

The simulation period covers the years 2002 and 2003 with 2002 as spin-up. Each participating model calculated the chemical state of the atmosphere for present day conditions using all emissions as described above. The perturbation simulations were performed by reducing the emission of each individual transport sector by 5% (see Table 3). This relatively small reduction was applied to avoid nonlinear responses of the chemical system which would occur by setting the respective emissions to zero. To check for linearity a final simulation was carried out with all transport sectors simultaneously reduced by 5%. Post processing confirmed the linearity of the small scale perturbation approach allowing to integrate the effects of the individual transport sectors in this setup.

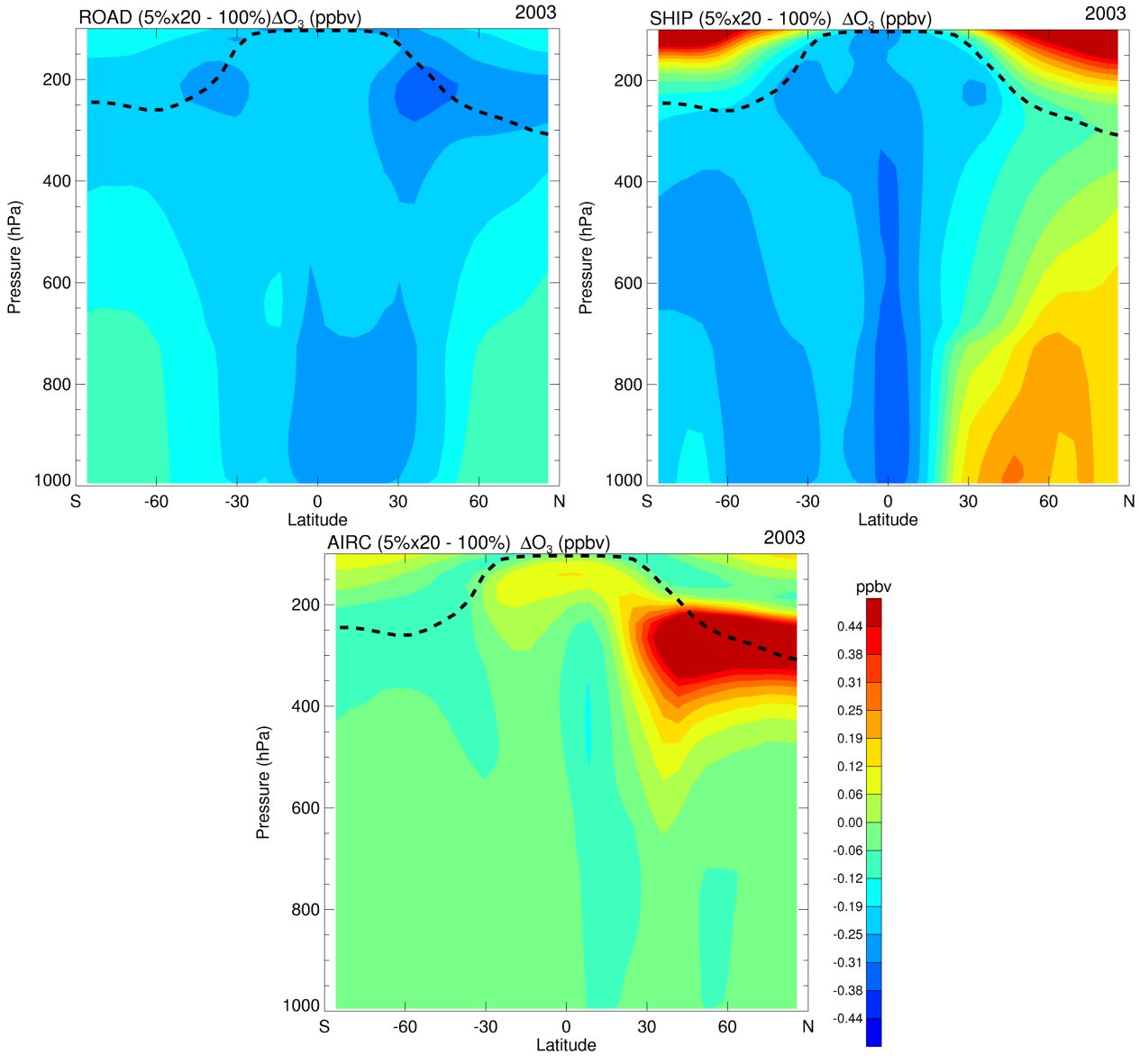

Fig. 2. Comparison of the small perturbation approach (5% emission reduction) and later scaling to a total removal of the respective traffic emission based on the simulations of p-TOMCAT. The plots indicate the difference of the ozone perturbation from both approaches.

2.1 Small perturbations and scaling

As mentioned above, for this study a small perturbation-approach was chosen for two main reasons: Since one focus of the analysis is a direct comparison of the impact of the differnt emissions, one needs to minimize non-linearities in the chemistry calculations. The total removal of one emission source could lead to responses of the chemical system such that the sum of the effects of each individual transportation sector exceeds the effect of all traffic emission sources switched off simultaneously. Furthermore the unscaled response of the chemical system is expected to be closer to the effect of realistic emission changes rather than a total emission decline.

We need to emphasize that the small scale approach is fundamentally different from a 100% perturbation, since non-linearities can lead to significant differences between both approaches. This is illustrated in Fig.2, which shows the differences of the ozone perturbations from a small perturbation approach, which is subsequently scaled to 100% and a 100% decline of the emissions. The sensitivity study was performed by one of the participating models (p-TOMCAT). It clearly shows that depending on the region where the emissions occur the effects are very different and can even have opposite signs.

The non-linearity with respect to aircraft emissions is mostly positive throughout the northern upper troposphere (i.e. the scaled small NO_x reduction leads to a stronger

Table 4. Participating models.

Model	TM4	p-TOMCAT	OsloCTM2	LMDzINCA	UCI-CTM	E39/C
Operated	KNMI	UCAM-DCHEM	UiO	LSCE	UCI	DLR
Model Type	CTM	CTM	CTM	CCM (nudg)	CTM	CCM
Meteorology	ECMWF OD	ECMWF OD	ECMWF OD	ECMWF OD	ECMWF OD	–
Hor. Resolution	$2^\circ \times 3^\circ$	T21	T42	$3.75^\circ \times 2.5^\circ$	T42	T30
Levels	34	31	40	19	37	39
Model Top(hPa)	10	10	10	3	2	10
Transport Scheme	Russel-Lerner	Prather	Prather	van Leer	Prather	Williamsen and Rasch
Convection	Tiedke	Tiedke	Tiedke	Tiedke	Tiedke	Tiedke
Lightning	Meijer et al. (2001)	Price and Rind	Price and Rind	Price and Rind, modified	Price and Rind	Grewe et al. (2001)
Transp. Species	26	35	76	66	28	12
Total Species	42	51	98	96	38	37
Gas phase reactions	68+16	112+27	163+47	291+51	90+22	107
Het. reactions	2	1	7	4	0	8
Strat. Chem.	no	no	yes	no	LINOZ	yes
NMHC Chemistry	yes, CBM4	yes	yes	yes	yes	no
Lightning NO_x(TgN/yr)	5	5	5	2	5	5
References	van Noije et al. (2006a,b)	O'Connor et al. (2005)	Gauss et al. (2003), Isaksen et al. (2005)	Hauglustaine et al. (2004), Folberth et al. (2005)	Wild et al. (2003), Hsu et al. (2005)	Grewe (2007), Dameris et al. (2005)

response of ozone compared to a total decline of the aircraft NO_x-source). The largest difference in that region occurs where the aircraft NO_x-source is located. As shown by Meilinger et al. (2001) the ozone production efficiency (PO3) in the upper troposphere is at maximum for NO_x levels around 1 ppbv. At NO_x levels of 0.1–0.3 ppbv, which are typical for this region, PO3 and thus the scaled ozone perturbation is more sensitive to a small decrease of NO_x than for a total removal of the aircraft NO_x source.

In contrast, the average effect of road traffic is of opposite sign. As will be shown below its effect on ozone in the upper troposphere can be quite substantial. Since road traffic emissions largely occur over the continents in regions with high background pollution and NO_x-levels in the ppbv-range, a small reduction of the emission enhances PO3. Therefore the scaled ozone perturbation from the small perturbation is larger than that from the total road perturbation. Vertical transport by convection over the continents, particularly during summer, redistributes this ozone perturbation to the tropopause region. It is interesting that the ozone response rather than the NO_x-perturbation from road is redistributed via convection in the models.

The sensitivity of ozone perturbations related to ship emissions is more complex. In the lower northern hemisphere troposphere NO_x-levels are generally found to be higher than in the tropics or southern hemisphere. Therefore the northern hemisphere troposphere responds most sensitively to small scale perturbations of the ship emissions.

The sensitivities deduced from p-TOMCAT are most likely at the higher end and differences between both approaches can expected to be smaller based on case studies from other models for individual sectors. Nevertheless one should keep in mind, that the small scale approach is fundamentally different from a total decline of one emission source.
In the following all perturbations are shown unscaled unless explicitly mentioned.

3 Participating models

Six models were applied to estimate the effect of traffic emissions on the current atmospheric chemical composition. Five of them simulated a two years period and included higher order chemistry schemes. These five models contribute to the ensemble mean results, which are presented in the following (TM4, p-TOMCAT, OsloCTM2, UCI and LMDzINCA). One model (E39/C) was used in a different mode to provide information on the interannual variability of the traffic impact using a ten year transient simulation. Four models are CTMs using prescribed operational ECMWF data to simulate the meteorological conditions (TM4, p-TOMCAT, OsloCTM2 and UCI). The other two models are coupled CCMs (chemistry climate models). LMDzINCA was nudged to the operational ECMWF fields whereas E39/C was operated as a climate model. Some general properties of the models are listed in Tab. 4. Except for E39/C all models included explicit NMHC chemistry. The TM4 uses a Carbon Bond Mechanism reaction scheme (CBM4) not including acetone chemistry. Three of the models do not include stratospheric chemistry reactions (TM4, p-TOMCAT, LMDzINCA). The number of species ranged from 42 (TM4) to 125 (LMDzINCA). LMDzINCA and TM4 used their own biogenic and oceanic emissions, respectively (see below).

3.1 TM4

The KNMI chemistry transport model TM4 (van Noije et al., 2006a,b) is driven by ECMWF analysed meteorology and contains a chemistry scheme derived from the Carbon Bond Mechanism reaction scheme (CBM4) (Houweling et al., 1998). It was run at a horizontal resolution of 2×3 degrees with 34 model levels from the surface up to 10 hPa.
The lightning parameterisation (Meijer et al., 2001) uses convective precipitation from ECMWF to describe the horizontal distribution of lightning and normalised profiles

calculated by Pickering et al. (1998) to distribute lightning produced NO_x vertically between cloud base and cloud top. Vertical emission profiles were also adopted as included in the respective emission files. In addition to the QUANTIFY emissions oceanic emissions were taken from the POET emission inventory, ammonia emissions from EDGAR 2.0, and volcanic SO_2 and DMS (Dimethylsulfide) emissions from the standard model configuration of TM4.

3.2 LMDzINCA

The CNRS-LSCE model, LMDz-INCA had a resolution of 3.75° in longitude and 2.5° in latitude with 19 levels extending from the surface up to about 3 hPa and is driven by ECMWF operational data (Hauglustaine et al., 2004).

The NMHC setup of the LMDz-INCA model was used. It considers detailed tropospheric chemistry with a comprehensive representation of the photochemistry of nonmethane hydrocarbons (NMHC) and volatile organic compounds (VOC) from biogenic, anthropogenic, and biomass burning sources.

Most anthropogenic emissions were taken from the EDGAR3.2FT2000 database. The effective injection height of biomass burning emissions into the atmosphere was taken into account with the emission heights calculated in the RETRO (REanalysis of the TROpospheric chemical composition over the past 40 years) project. The lightning source was determined interactively in LMDz-INCA with a modified Price and Rind (1992) parameterization, and its total was prescribed at $\approx$ 2. Tg[N]/year. Biogenic sources were calculated with the vegetation model ORCHIDEE. Oceanic emissions were taken from Folberth et al. (2005).

3.3 OsloCTM2

The Oslo CTM2 model is a 3-D chemical transport model driven by ECMWF meteorological data and extending from the ground to 10 hPa in 40 vertical layers. The horizontal resolution for this study was Gaussian T42 (2.8°×2.8°). The model was spun up for several years with emissions from the POET and RETRO projects, then for additional 6 months with the emissions provided for the QUANTIFY project. One restart file was archived for March 2002. From this file the five different scenarios were started, which were run for 22 months.

3.4 p-TOMCAT

The model used during the first part of the QUANTIFY project is the global offline chemistry transport model p-TOMCAT. It is an updated version (see O'Connor et al. (2005)) of a model previously used for a range of tropospheric chemistry studies (Savage et al., 2004; Law et al., 2000, 1998). Convective transport was based on the mass flux parameterization of Tiedtke (1989). The parametrizations includes descriptions of deep and shallow convection with convective updrafts and largescale subsidence, as well as turbulent and organized entrainment and detrainment. The model contains a nonlocal vertical diffusion scheme based on the parameterization of Holtslag and Boville (1993).
In this study p-TOMCAT was run with a $5.7^o \times 5.7^o$ horizontal resolution and 31 vertical levels from the surface to 10 hPa. The offline meteorological fields used are from the operational analyses of the European Medium Range Weather Forecast model. The chemical mechanism includes the reactions of methane, ethane and propane plus their oxidation products and of sulphur species, it includes 96 bimolecular, 16 termolecular, 27 photolysis reactions and 1 heterogeneous reaction on sulphuric acid aerosol. The model chemistry uses the atmospheric chemistry integration package ASAD (Carver et al., 1997) and is integrated with the IMPACT scheme of Carver and Scott (2000). The ozone and nitrogen oxide concentrations at the top model level are constrained to zonal mean values calculated by the Cambridge 2D model (Law and Nisbet, 1996). The chemical rate coefficients used by p-TOMCAT have been recently updated to those in the IUPAC Summary of March 2005. The model parameterizations of wet and dry deposition are described in Giannakopoulos et al. (1999).

3.5 UCI

The UCI CTM is a 3-D eulerian chemistry-transport model driven by meteorological data from the ECMWF IFS version cycle 29r2 at T42L40 (see OsloCTM2). Tropospheric chemistry is handled by ASAD software package (Carver et al., 1997), containing 38 species (28 transported) and 112 reactions (Wild et al., 2003), while in the stratosphere, it employs the stratospheric linear ozone scheme (Linoz) and conducts linear calculations of (P-L) (Hsu, 2004). Photolysis rates are calculated by the Fast-JX package (Bian and Prather, 2002). Transport scheme uses the second order moments (Prather, 1986). Lightning is parameterized with the method of Price and Rind (1992). Convection is simulated, following the ECMWF Tiedtke convection diagnostics.

3.6 E39/C

Impacts by road and ship traffic were provided by DLR based on simulations with E39/C. The perturbation fields are derived as monthly mean values from a transient simulation from 1990 to 1999 (Dameris et al., 2005; Grewe, 2007). The meteorology is calculated by the climate model ECHAM4.L39(DLR) and therefore does not represent an individual year. Nevertheless, it represents the late 20 century climate and is therefore to some extent comparable to the other simulations of the year 2003. In particular the emissions which were used by the other participating CTMs are different. The impacts are derived using tagging methods (Grewe, 2004) and hence differ from the 5% change approach used by other modelling groups in QUANTIFY.

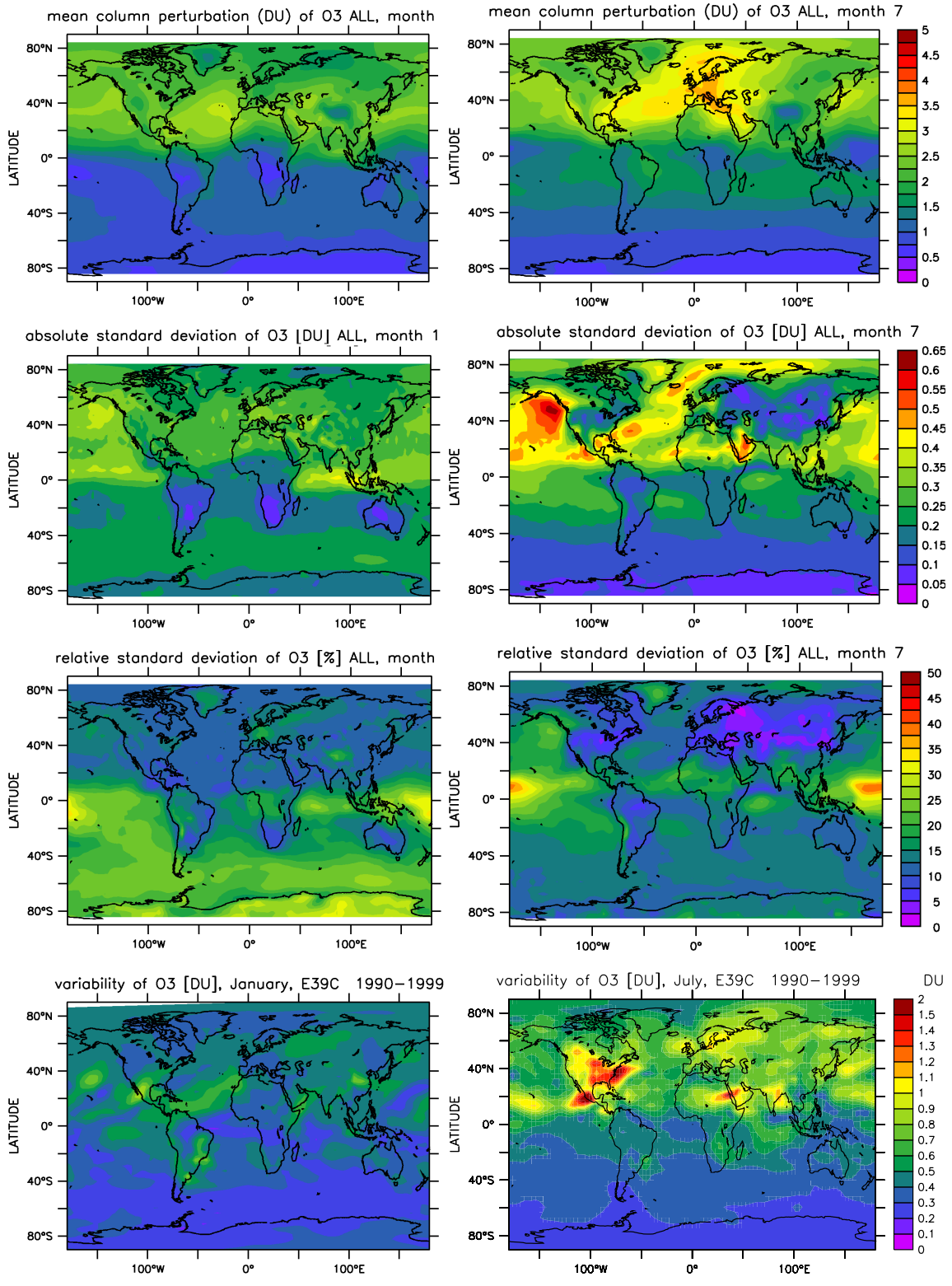

Fig. 3. Mean column ozone perturbations for the integrated emissions from all types of transport obtained from the average of TM4, LMDzINCA, OSLO CTM2, UCI and p-TOMCAT (top row) for January (left) and July (right). The corresponding absolute and relative standard deviations (relative to the ensemble mean perturbation) are displayed in the second and third row. The lower two panels show the interannual variation of the detrended transportation induced ozone perturbation based on E39/C. Note that the data on display are scaled to 100% to allow the comparison to the interannual variability deduced from E39/C.

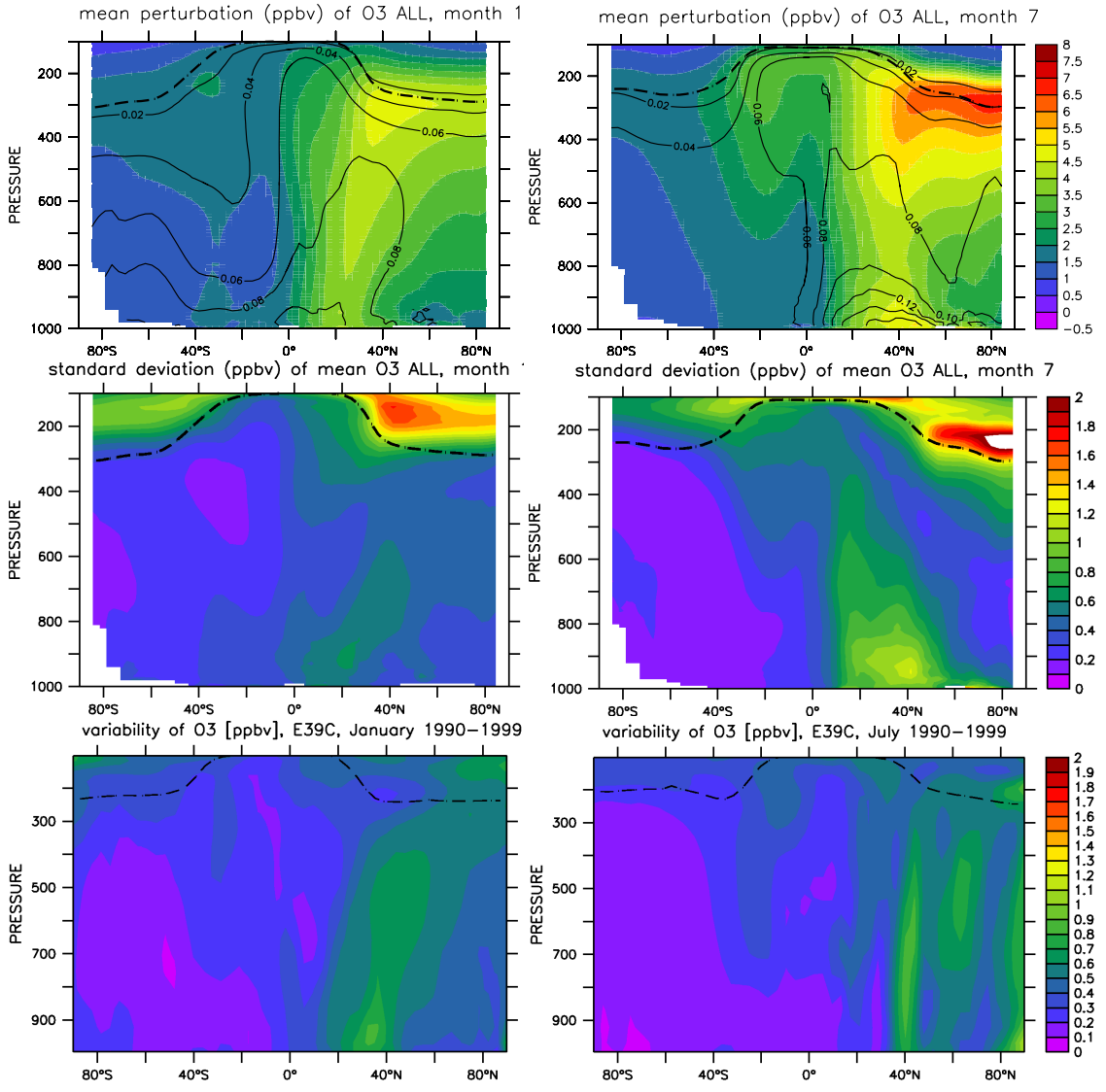

Fig. 4. As Fig. 3, but for the zonal mean in ppbv (scaled to 100%). Solid contours show the perturbation relative to the mean unperturbed simulation and the dashed line indicates the tropopause.

However, both methods try to identify the individual contributions from sectors. Changes in the contributions are detected comparably by both approaches (Grewe, 2004), i.e. the standard deviation based on interannual variability is similar for both approaches.

4 Traffic induced ozone changes

4.1 Total ozone perturbation

The integrated effect of the emission reduction (ALL-case) by 5% is shown in Fig. 3 for January and July, respectively. Note that the data in Figs. 3 and 4 are scaled to 100% to allow the comparison to the interannual variability of E39/C (see below). The column ozone distribution change was integrated from the surface up to 50 hPa. The results from E39/C are not included in the calculation of the mean fields since the results of E39/C were obtained with a different setup and a different method.

The mean total ozone perturbations in Fig. 3 exhibit strong hemispheric differences of the traffic emissions with almost zero effect in the southern hemisphere, but maximum effects of about 4 DU during northern hemisphere summer (3 DU during winter). All models simulate a similar location of the strongest ozone perturbation extending from the northern subtropical Atlantic to central Europe.

The maximum ozone perturbation is strongest pronounced during northern summer. Interestingly its southern hemispheric seasonal cycle – despite being weak – is in phase

with the northern hemisphere with a maximum effect of less than 2 DU. This is most likely due to interhemispheric transport and mixing of ship and road emissions occuring during northern summer, which exceed the effects of emissions on the southern hemisphere (see also Fig. 6).

Note furthermore that the effects of traffic emissions over the Pacific and Indian Ocean downwind of the densly populated coastal areas and sources of pollution, are not as strong as over the central Atlantic Ocean. A comparison with the NO_x emission distribution (Fig. 1) indicates that over the northern hemispheric Atlantic in particular ship traffic and also aircraft emit large amounts of NO_x and that these strong emissions occur over a relatively large area. Over the eastern US and western Europe the sum of all three emission categories reach a maximum. Their combination is responsible for the relatively strong perturbations in these regions.

To assess the robustness of the perturbation signal two tests are performed. First the model to model differences in terms of the associated standard deviation is assessed to estimate the impact of model uncertainties. Second, the impact of the chosen meteorology (year 2003) is tested by comparing to the interannual variability using the standard deviation of the transport signal derived from the transient E39/C simulation, which includes natural variability of the troposphere and the stratosphere due to variations of ozone influx, transport patterns (e.g. induced by El Nino), and others (Grewe, 2007). The inter-model standard deviations (one-σ) are shown in Fig. 3c–f. Overall the models calculate very similar patterns with a relative standard deviation mostly below 15% over large regions of the globe where the effect of the perturbation is strongest. In the southern hemisphere, the relative standard deviations are in general somewhat higher (between 20–30%), since the absolute column perturbations (Fig. 3c and 3d) are not as large as in the northern hemisphere. The large absolute deviation over the northern Pacific Ocean during July is caused by the impact of ship emissions, which leads to ozone perturbations ranging from 0.5 DU (TM4) to 2 DU (p-TOMCAT). Largest relative deviations occur over the tropical central Pacific, where perturbations of ozone are relatively low. Thus, small perturbations may lead to relatively large variations between the models. Note however, that calculated ozone perturbations in particular over Europe and the central Atlantic are relatively robust indicating a significant impact of traffic emissions in these regions.

To assess the interannual variability of the signal we compared the transport induced ozone changes to a ten year transient simulation of E39/C. As can be seen from Fig. 3(bottom) the traffic induced perturbation signal simulated by E39/C over the ten years period is on the order of 0.8 DU and 1.2 DU in January and July, respectively. Largest variations occur in coastal regions, where synoptic variability leads to advection of either relatively clean maritime air or air from polluted urban areas. Although the perturbation signal from E39/C is largest compared to the other models, the ensemble mean response of the models is still larger than the interannual variability of the transport induced ozone changes according to E39/C. Thus, focusing on a particular year is justified within a 10% uncertainty for ozone since this is the climatological variability simulated consistently within one model.

4.2 Zonal mean ozone perturbation

The zonal mean ozone perturbation for the integrated traffic emissions (Fig. 4) shows the largest effect in the northern subtropics/lower-middle latitudes. In the northern hemisphere boundary layer the mean ozone perturbation peaks at 5.5 ppbv in mid latitudes at 40–50°N during summer decreasing to less than 3 ppbv during winter. The perturbation mixing ratio peaks in the upper troposphere/lower stratosphere of the northern extratropics during summer, largely due to aircraft emissions as will be seen later (Fig. 5).

The relative perturbation in the upper troposphere is of the order of 4–6% during January and July. However, as indicated in Fig. 4 the strongest relative effect can be as large as 16% in the northern hemisphere boundary layer during summer. During winter the perturbation peaks at 10% and is located in the tropical boundary layer.

For the southern hemisphere the models calculate the strongest absolute effect on the ozone mixing ratio also for the upper troposphere, although the changes relative to the unperturbed case maximize in the marine boundary layer. In the southern hemisphere, both, absolute and relative changes are about 50% lower than in the northern hemisphere. The effect on ozone in the southern boundary layer is only about 2 ppbv during January and July.

As illustrated in Fig. 4 largest uncertainties between the models are found near the tropopause and during summer when convection plays an important role in vertical transport in particular in the northern extratropics. Large emissions by traffic take place in that latitude belt and thus have the highest probability to be redistributed from the surface to higher altitudes via convection during the summer months. The associated variations between the individual models in that region range from 3.5 ppbv (LMDzINCA) to 6 ppbv (p-TOMCAT) at 250 hPa during July resulting in a standard deviation of 2 ppbv. In the extratropics of the southern hemisphere the effect of summer convection is not as pronounced due to the hemispheric differences of the emissions.

Interestingly, the interannual variability of the zonal mean ozone perturbations of around 0.5 ppbv ($\approx$5%) for both January and July, is much smaller than the variations between the models ($\approx$20%). The latter can be explained by the different convection schemes and grid resolutions, which introduce large uncertainties to the distribution of the chemical species (Tost et al., 2006, 2007). However, the rather small interannual variability also indicates that year-to-year changes of meteorology lead to changes in the horizontal distribution of ozone perturbations and the location of convection. The effect of vertical transport and

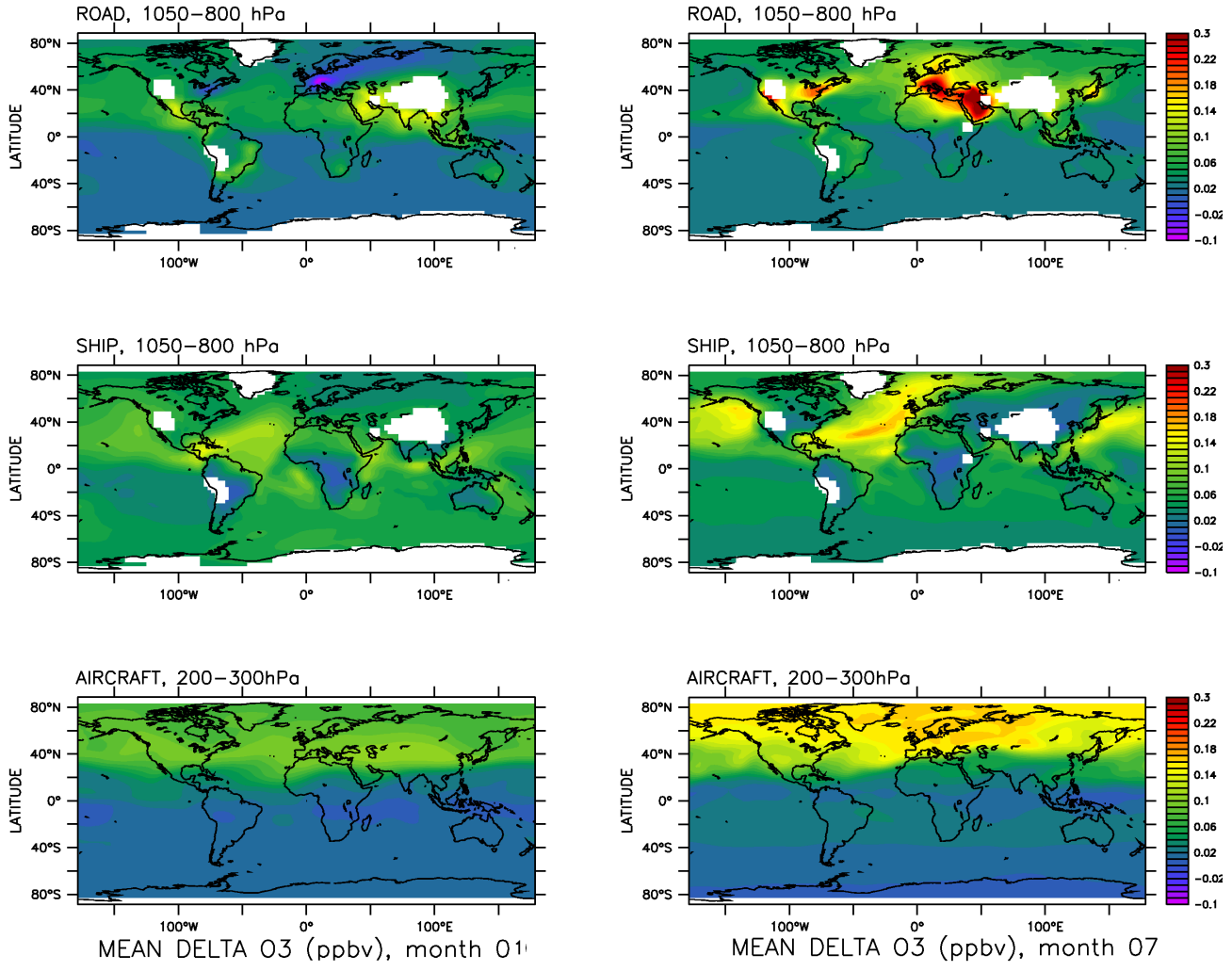

Fig. 5. Mean perturbations of ozone (ppbv) in the lower troposphere (surface-800 hPa) during January (left column) and July (right) for the different modes of transportation applying a 5% emission reduction. The values for aircraft are shown for 300–200 hPa.

mixing within one model differs less, although horizontally displaced.

4.3 Effects by transport modes

The effects of the emissions from road, ship and aircraft on ozone are shown in Figs. 5–6 for January and July, respectively. The results indicate that the road emissions have the strongest effect on ozone in the summer boundary layer over the eastern US and central Europe extending over the Mediterranean to the Arabian Peninsula (Fig. 5). During winter the average effect of road traffic on ozone in the highly industrialized regions of the extratropics almost vanishes or even changes sign, i.e. an increase of road emissions leads to a decrease of ozone during winter. Often under stable boundary layer conditions the emissions accumulate, on average to more than 2 ppbv over the industrialized centers over the eastern US, Europe and parts of East Asia (not shown). Under these conditions additional NO_x from (road) traffic locally leads to the titration of ozone. In addition the ozone production efficiency can be increased by reduced NO_x emissions under high NO_x conditions leading to a higher ozone productivity per emitted NO_x.

Matthes et al. (2007) and Niemeier et al. (2006) find larger relative ozone perturbations due to road traffic of about 10% for some regions in the northern hemisphere boundary layer performing similar model simulations. Part of the deviations to our results can be explained by the use of different emissions, which are based on the EDGAR 1990 fuel estimates in Matthes et al. (2007) and are about 25% higher for NO_x from road than in this study. The inverted sensitivity of ozone to road emissions during winter is also reported by Niemeier et al. (2006) with the maximum effect over Europe exceeding 25% at the surface. The latter effect is simulated by all five models in our study, which contribute to the average shown

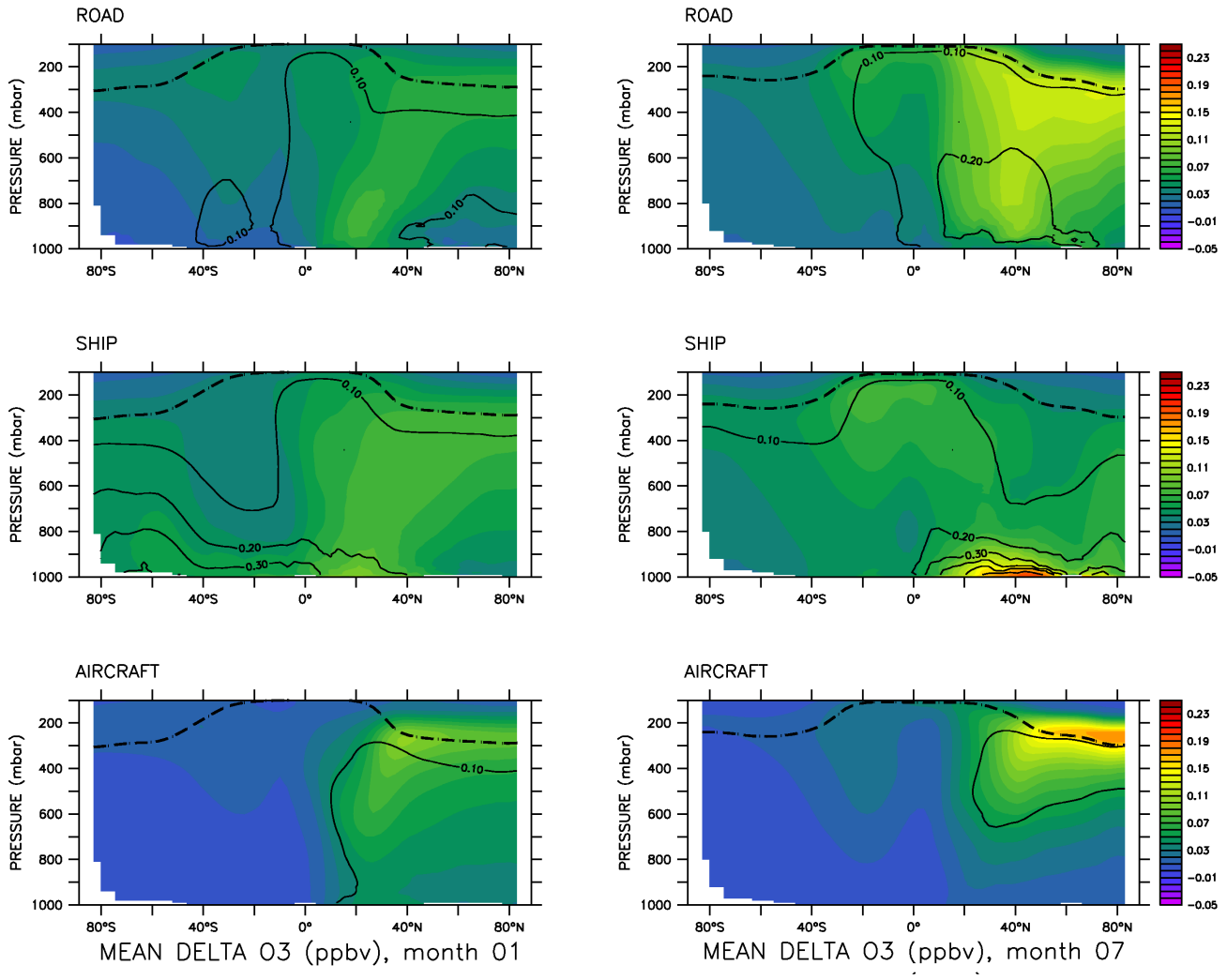

Fig. 6. Same as Fig. 5, but for the zonal mean ozone perturbation. Solid contours show the change relative to the base case simulation, dashed line indicates the tropopause.

in Fig. 5. Quantitatively, the results of Niemeier et al. (2006) also exceed our calculations by a factor of 2–3 at the surface when scaling our results to 100%. However, since Niemeier et al. (2006) removed the road traffic emissions completely their larger response of ozone is not inconsistent with our results.

Ship emissions have a significant impact throughout the year also with a maximum in July over the central Atlantic/western European region. In the northern hemisphere their effect dominates the boundary layer perturbation during January and July. Over the northern Pacific region mainly the emission from ships contributes significantly to the ozone perturbation, whereas the North Atlantic region additionally is affected by road emissions, which are transported efficiently from the highly polluted Eastern US to the Atlantic.

Not too surprising, in the northern UTLS region (upper troposphere / lower stratosphere) the effect of aircraft emissions dominates the ozone perturbation (Fig. 6) being approximately half as large during January compared to July associated with the enhanced level of photochemistry. The ozone perturbation from road traffic during summer is even higher than the perturbation due to aircraft emissions in winter, highlighting the role of road traffic for the chemical state of the UTLS in summer (see also Fig. 7). Ship emissions, despite of the high importance in the July boundary layer (Fig. 5) do not show a similar effect in the UTLS, indicating that convective and large scale transport from the marine boundary layer do not have the same impact as continental convection for road traffic.

This is also evident from Fig. 7, which shows the temporal evolution of the ozone perturbations for the different modes of transport. Comparing ship and road induced ozone perturbations ship emissions have a larger impact on boundary layer ozone than road traffic over the whole year. In the

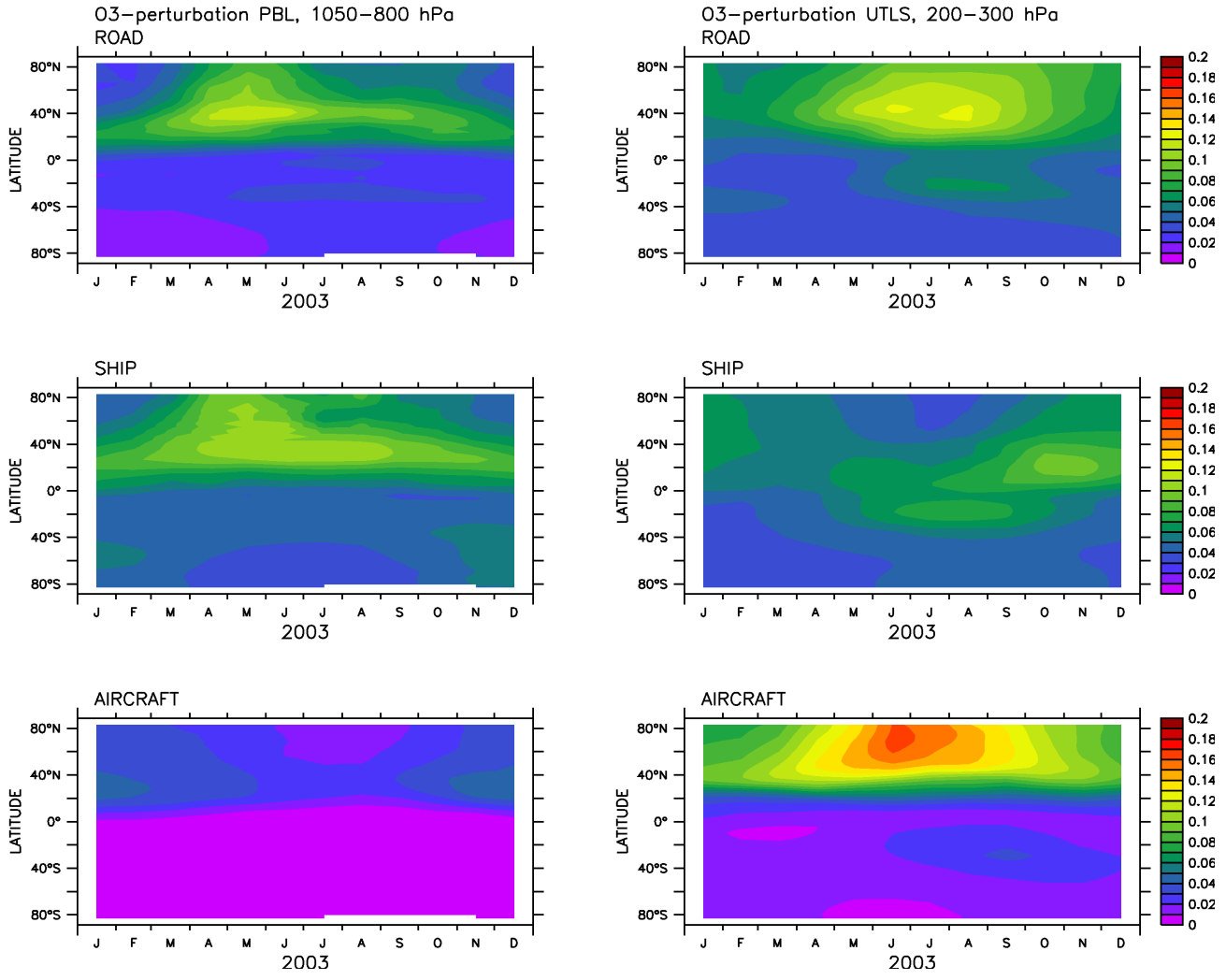

Fig. 7. Temporal evolution of the zonal mean ozone perturbation in ppbv (based on 5% traffic emission change) for the lower troposphere (left column) and the UTLS region (right).

upper troposphere and lower stratosphere the ozone perturbation from road traffic peaks in summer over in the northern mid latitudes exceeding the effect on the boundary layer. The effect of ship emissions does not exhibit this strong seasonal signal in the upper troposphere although their effect on surface ozone shows a similar zonal and temporal distribution as for road.

Globally the effect of ship emissions on ozone in the boundary layer is larger than those from road emissions, whereas both are almost equal in the upper troposphere (Table 5). Notably in the upper troposphere aircraft emissions do not dominate the annual mean global effect between 200–300 hPa. Their influence is rather concentrated to latitudes poleward of 30° N (see Fig. 6) whereas road and ship traffic affect the UT globally. Therefore Table 5 also lists the ozone perturbations for the latitude band 30°–60° N. In the northern upper troposphere aircraft emissions on average account for 1.63% (scaled) to the ozone changes between 30°–60° N with maximum ozone perturbations of 4.2% (scaled). These values are lower than reported by Schumann (1997) and slightly less than in Gauss et al. (2006). A possible reason for the discrepancies are the different model resolutions since in those studies the applied resolutions coarser than 3.75°×3.75° (Schumann, 1998) or T21 (Gauss et al., 2006). The model with the lowest resolution (p-TOMCAT) in our study also calculates the strongest average perturbations which are in the range of 150–232.5 pptv (or 1.6–4.2% when scaling to 100%) with maxima during summer exceeding 300 pptv. The coarse resolution leads to an instantaneous spread of the emissions over large areas and volumes which artificially dilutes the NOx and increases the ozone response. Despite the lower model resolution, Kentarchos and Roelofs (2002) obtained similar results as in our study, but they used 15% lower emissions, which could further indicate that a low resolution tends to yield stronger perturbations.

Table 5. Globally averaged ozone perturbations (unscaled) by transport mode for the lower and upper troposphere in pptv. Also given is the maximum percentage change relative to the unperturbed case. Scaled percentage values are give in italics. The analysis is also shown for the latitude band of 30°–60° N indicating zonal mean as well as maximum perturbations (note that the relative and absolute perturbations can occur at different locations resulting in different orders between the transportation sectors).

global		1000–800 hPa				300–200 hPa		
	MEAN	σ	%	scaled	MEAN	σ	%	scaled
ROAD	−43.5	11.0	−0.14	*−2.89*	−58.5	15.0	−0.047	*−0.95*
SHIP	−60.0	13.0	−0.20	*−3.99*	−56.0	10.5	−0.045	*−0.91*
AIR	−15.0	3.5	−0.05	*−1.0*	−44.5	23.0	−0.036	*−0.72*
ALL	−118.5	22.0	−0.39	*−7.9*	−160.	28.5	−0.13	*−2.61*
30°–60° N	1000–800 hPa				300–200 hPa			
ROAD, mean	−77	20	−0.18	*−3.66*	−89.5	21.0	−0.075	*−1.5*
SHIP, mean	−83.5	18	−0.22	*−4.47*	−61.0	11.5	−0.05	*−1.0*
AIR, mean	−32	9	−0.08	*−1.63*	−108.	45.0	−0.08	*−1.63*
ROAD, max	−334.5	–	−0.57	*−11.41*	−172.	–	−0.21	*−4.23*
SHIP, max	−265.5	–	−0.95	*−18.9*	−136.	–	−0.28	*−5.51*
AIR, max	−69.0	–	−0.15	*−3.06*	−184.5	–	−0.22	*−4.31*

In addition, plume processes are not captured at all in the models, which may lead to additional uncertainties. Modifications of the emissions through e.g. heterogeneous chemistry on contrails may lead to enhanced ozone destruction (Meilinger et al., 2005). The recently published update of the reaction of NO with HO_2 (Cariolle et al., 2008) would lead to a stronger conversion of NO_x to HNO_3 removing more aircraft-NO_x from the active phase. On the other hand HNO_3 acts as a reservoir species particularly in the lower stratosphere, which could compensate for this effect. Lightning NO_x is unlikely to have caused the differences since there is no systematic difference between the 5 TgN/yr in our study and previous investigations.

Our findings are also evident in the vertical zonal mean cross sections (Fig. 6), highlighting the importance of surface emissions from ship and road traffic for the tropical upper troposphere. It also shows that the impact of road traffic is of larger importance for the extratropical troposphere in the northern summer hemisphere (see also Table 5). In the tropics ship emissions are the strongest contributor to the ozone perturbation in the tropical transition layer (TTL), being of greater importance than aircraft emissions there. As evident from Fig. 6 the impact of road and ship emissions seems to influence the whole TTL region from 20° S–20° N in particular during northern summer. During January, when the Inter Tropical Convergence Zone (ITCZ) is located in the southern hemisphere, where the emissions are much lower, the TTL is only weakly affected. Note also that for the upper troposphere in the southern hemisphere the effect of ship emissions is among all modes of transport the strongest contributor in January as well as in July (comp. also Fig. 7).

4.4 Relative importance of traffic sectors

In addition to the perturbation of O_3 the contribution of each individual transport sector relative to the total effect from traffic is of interest. As shown in Fig. 8 the relative impact of road and ship emissions differ substantialy although both are released at the surface. In the region between the surface and 900 hPa the relative effect of ship emissions clearly dominates the total perturbations by all traffic emissions in each summer hemisphere. In the southern hemisphere during January the perturbations of ship emissions can almost contribute up to 85% of the total ozone perturbation, since ship emissions are the major source of pollutants south of 40° S. In the northern extratropics the effects from ships are most important in the boundary layer below 950 hPa, where the mean perturbation relative to the background can be as high as 16% (see also Fig. 8). As evident from Fig. 8 the contribution of ship emissions is particularly important in the subtropical monsoon regions and the tropics, where convection leads to upward transport of the emissions and to a relative contribution of 50% up to the tropical tropopause.

The relative contribution of road emissions peaks in the free troposphere in both summer hemispheres with a pronounced seasonal cycle in the northern extratropics. The maximum effect on ozone occurs in July, when convection at these latitudes is strongest. Thus during that time of the year pollutants from road traffic have a much higher probability to be transported to tropopause altitudes compared to winter. This is also evident from Fig. 6 where the ozone perturbations in July below the tropopause are almost equal to the effect from aircraft.

Note that ship emissions only weakly affect the free and upper troposphere of the northern extratropics during July.

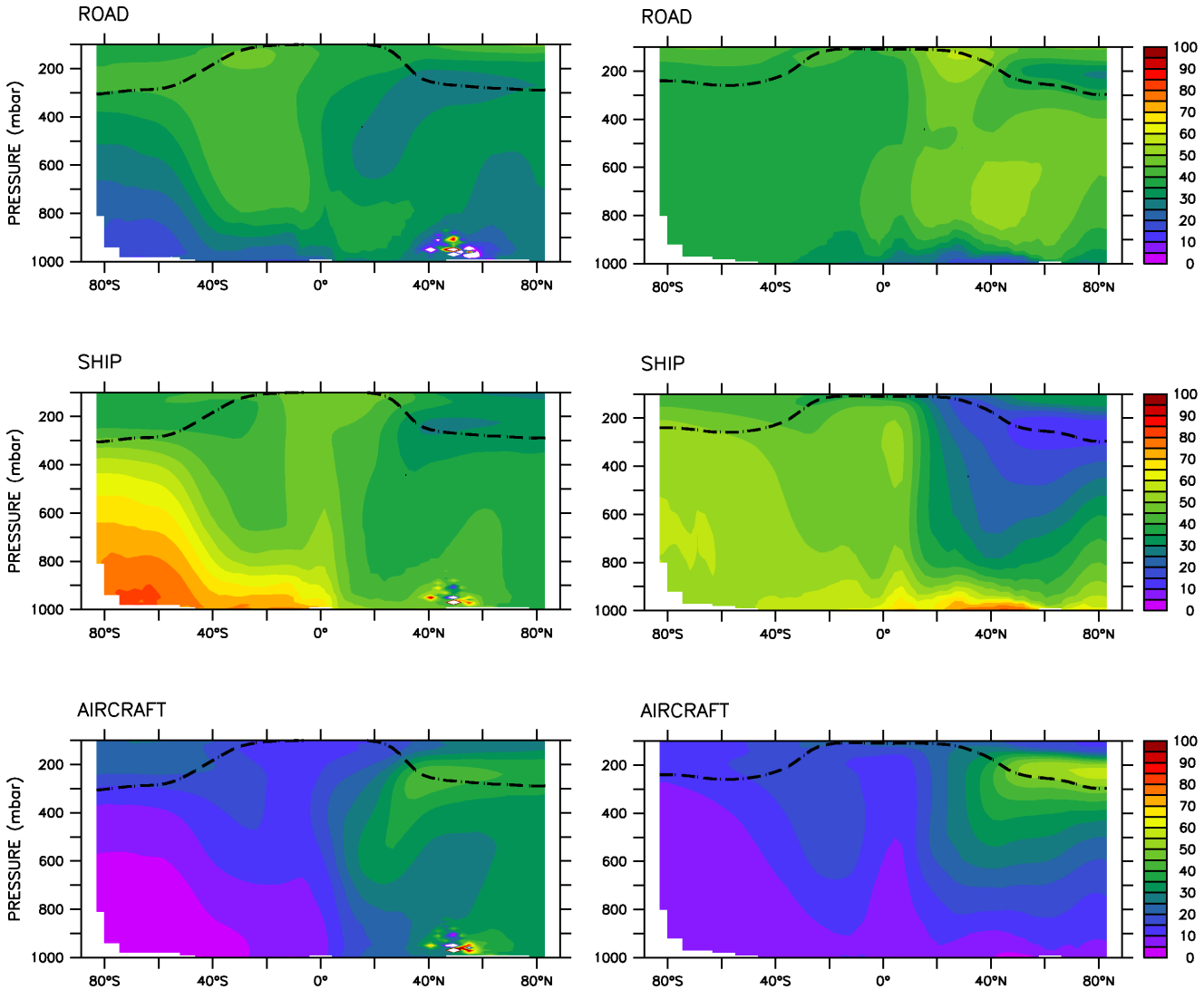

Fig. 8. Relative contribution of each transport sector to the total ozone changes due to the sum of emissions in all transport sectors for January (left) and July(right).

Since ships largely emit over the open oceans where convection is not as strong as over the continents, they have a much lower potential to reach the upper troposphere of the extratropics compared to road emissions. Therefore, in the winter hemispheres the effects of road and ship traffic on ozone show similar patterns (Fig. 6). As indicated by Fig. 8 the relative contribution of road traffic on the free and upper extratropical troposphere is about 15% larger than that of ships. Directly at the tropopause and in the lower stratosphere the contribution of aircraft dominates in the northern hemisphere, whereas in the southern hemisphere upper troposphere its effect on ozone is the smallest of the three types of traffic.

Note also that the relative contributions as given in Fig. 8 are based on the small emission perturbation and therefore the relative fractions of each sector are different from the entire removal of each emission source. However, the sensitivities as calculated here are expected to be more realistic in view of actual emission changes based on mitigation policies than a total decline of the sources.

Table 6. Global annual average ozone burden change per annual integrated NO_x-emission of each respective transport sector in molecules(ΔO_3)/molecules(NO_x-emission)

	TM4	OSLO	LMDz	UCI	p-TOM	mean	σ
ROAD	0.31	0.44	0.34	0.35	0.26	0.33	0.05
SHIP	0.47	0.65	0.46	0.57	0.57	0.54	0.07
AIR	1.32	1.22	1.45	1.39	2.78	1.63	0.58

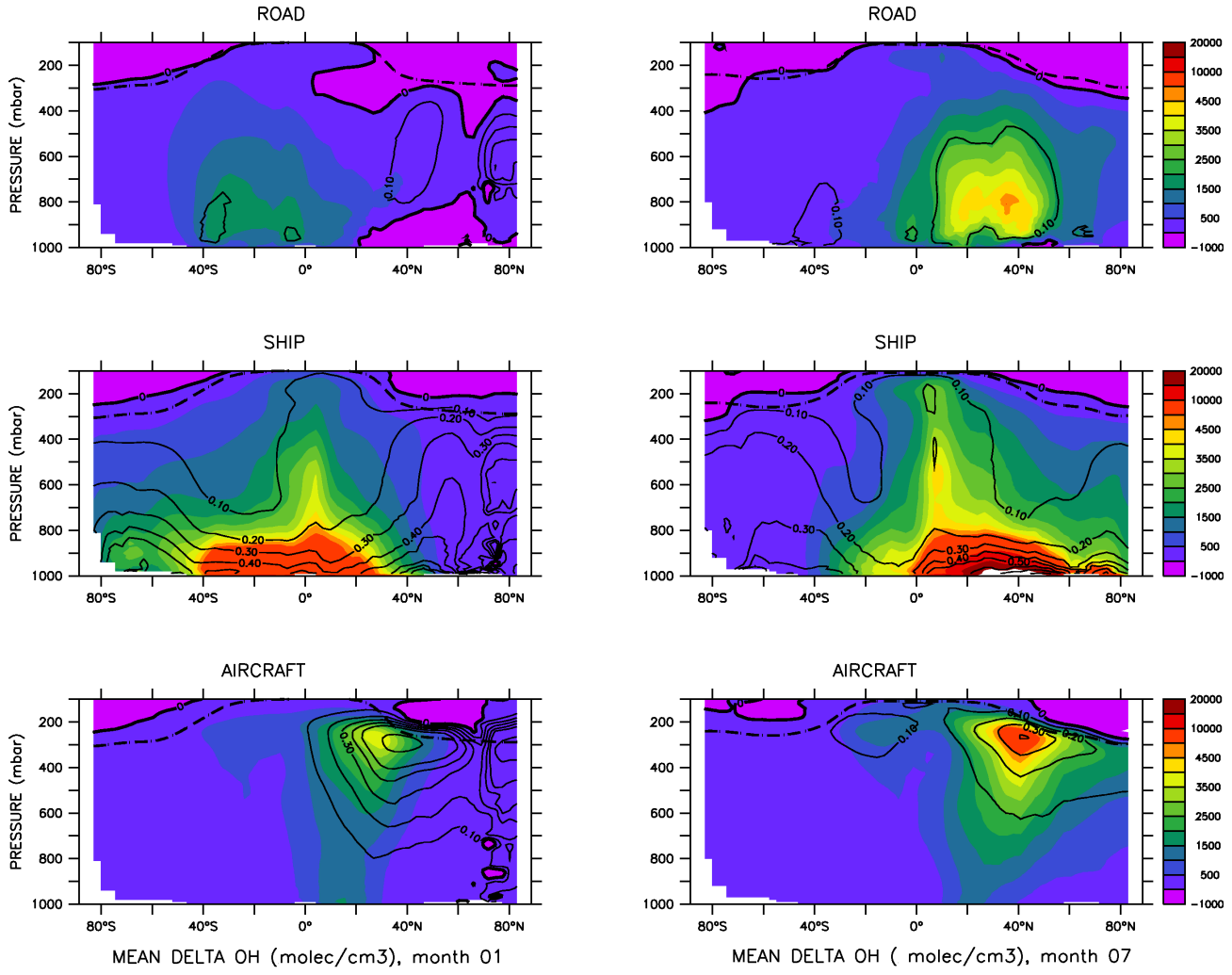

Fig. 9. Zonal mean OH perturbation for January (left) and July for a 5% perturbation of road (top), ship (middle) and aircraft (bottom) emissions, respectively (shading). Contours show the perturbation relative to the base case simulation.

To estimate the efficiency of the ozone perturbation from each transport sector we normalised the additional annual mean ozone burden of each sector to the respective number of NO_x molecules emitted. As evident from Table 6 road and ship emissions have similar efficiencies to perturb ozone. However, the NO_x emissions from air traffic are almost three times as efficient in producing ozone as those from ships. Since these emissions take place in the UTLS region the lifetime of the reservoir species HNO_3 and PAN are much longer than at the surface. Therefore each NO_x molecule can be recycled more often to produce ozone before being removed via precipitation scavenging and dry deposition of HNO_3.

Note that despite some individual differences, all models indicate the largest efficiency to perturb ozone for NO_x emissions from aircraft and the weakest efficiency for road traffic. Ship emissions occur largely in remote areas with much lower background pollution compared to road emissions. In these remote marine regions ozone is more sensitive to NO_x-perturbations compared to the polluted land regions, where most of the road emissions are released.

5 OH

5.1 Global OH

The effects of different transport systems on tropopspheric OH concentrations are shown in Fig. 9 for January and July, respectively. Interestingly, ship emissions have the largest impact on the global OH budget in the boundary layer. During northern summer the effect of NO_x from maritime traffic on OH can be as large as $2.5{\cdot}10^4$ molecules/cm^3 at 40° N equivalent to an increase of up to 0.8% (or $5{\cdot}10^5$ molecules/cm^3 and 15%,respecively, when scaling to 100%). During winter the effect of ship emissions is about a

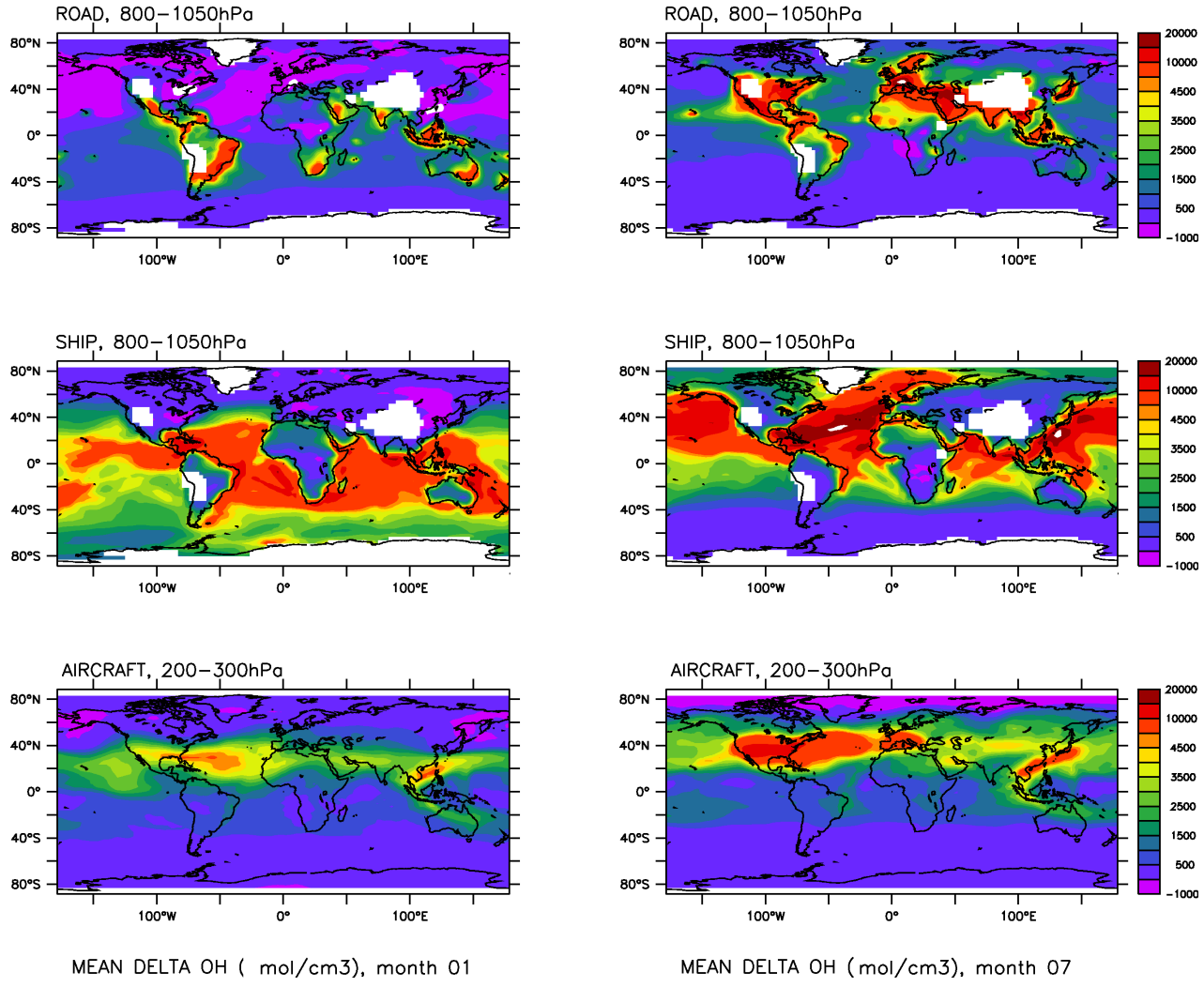

Fig. 10. Mean OH perturbation (5% traffic emission reduction) in the boundary layer during January (left) and July (right) between 800-1000 hPa for road- (top) and ship emissions (middle). The effect of aircraft emissions is displayed for 200–300 hPa (bottom).

factor of two lower, thereby reaching a maximum in the latitude band from 40° S to 30° N. Since the OH concentrations are globally highest in these regions, a (scaled) increase by about $5{\cdot}10^5$ molecules/cm^3 is of similar magnitude as the annual mean concentration in temperate and high latitudes, and is therefore highly significant on a global scale. Also in winter the boundary layer OH perturbation is still of the order of 10%. As can be seen from Fig. 9 ship emissions are dominating the annual zonal mean OH perturbation in the boundary layer throughout the year.

The effect of road emissions on the OH distribution shows a pronounced seasonal cycle in particular in the northern hemisphere. The maximum effect occurs during northern summer in the continental boundary layer between 800–900 hPa reaching $5{\cdot}10^3$ molecules/cm^3 or about 0.18% (zonal annual mean). Since road emissions are largely emitted in polluted industrialized regions over the continents the zonal mean effect on OH at 1000 hPa is less pronounced than at 900 hPa. High NO_x-levels make OH less sensitive to perturbations as further explained below. However, in particular during northern summer road transport seems to be most important for the lower troposphere in the extratropics up to 500 hPa.

The horizontal distribution (Fig. 10) reveals that the effect on a regional basis can be much stronger than $5{\cdot}10^3$ molecules/cm^3. The largest impact is found in the industrialized regions of the Eastern US, central Europe and East Asia reaching $2.5{\cdot}10^4$ molecules/cm^3. In these regions OH has the highest potential to be recycled via the reaction of NO with HO_2, which is produced after the initial reaction of OH on the carbon containing reactive species (e.g. CO, CH_4, NMHCs). The additional NO_2 from this reaction in turn leads to the enhanced formation of ozone and OH production via $O^1(D)$. During winter the emissions of CO and

Table 7. Methane lifetime in years for the BASE case and relative changes due to a decrease of traffic emissions of 5%. Scaled mean values are given in italics. Top boundary for the integration was 50 hPa. Note that no feedback factor is included.

	TM4	OSLO	LMDz	UCI	TOMCAT	mean	σ	scaled	σ
BASE (yr)	7.23	8.49	10.23	7.45	11.43	8.97	1.63	*8.97*	*1.63*
ROAD (%)	0.093	0.068	0.096	0.064	0.081	0.805	0.013	*1.61*	*0.25*
SHIP (%)	0.162	0.185	0.206	0.176	0.320	0.206	0.05	*4.12*	*1.02*
AIR (%)	0.041	0.032	0.053	0.047	0.09	0.052	0.02	*1.04*	*0.40*

NMHCs in these regions act as a direct sink, since solar radiation is reduced.

Comparing the impact of road and ship traffic, both surface sources of air pollution, the effects on OH are very different, although the annual amount of emitted NO_x is similar (see Table 1). The zonal mean perturbation of road emissions peaks at about 0.2% during northern summer and 0.1% in the southern hemisphere summer. The regional effect during July can exceed 0.5% in the continental boundary layer for road traffic. As evident from Fig. 9 ship emissions have a larger effect even in the zonal mean. The large differences of both means of transportation on OH can be related to the different regions and pollution conditions. As will be seen later, the sensitivity of OH to traffic emissions is largest in the still relatively pristine regions over the (sub-)tropical oceans. Background concentrations of ozone, NO_x and other NMHCs are low, and the solar irradiation and water vapor available for OH formation are high. The recycling potential of OH by NO_x is lower than over the continents and is efficiently enhanced by ship emissions. The reason is that at already enhanced NO_x levels the reaction of OH with NO_2 becomes a significant sink of hydroxyl radicals, which is not the case in the NO_x-poor marine boundary layer. On the other hand these low NO_x concentrations accompanied with high OH make the system more sensitive for NO_x perturbations than in polluted areas (Lelieveld et al., 2002). Furthermore, road emissions occur at higher altitudes and latitudes where average water vapor concentrations and solar irradiation are lower and in regions where other anthropogenic sources of pollution cause enhanced NO_x levels. The combination of these factors leads to a lower sensitivity of OH to perturbations from road traffic than for ship emissions.

The regional perturbation pattern (Fig. 10) illustrates that locally the effects of road and ship emissions on OH are similar during northern summer. The strongest effect is simulated for the ship emissions over the northern subtropical Atlantic in the same region where also ozone exhibits the largest perturbation (see Fig. 5). Note furthermore that in particular during northern summer the effect on OH at high northern latitudes over Europe is as high as over the eastern subtropical Pacific. Thus the increasing ship traffic at high northern latitudes as a response to the diminishing ice coverage due to the relatively rapid climate change (Lemke et al., 2007, IPCC) might have strong effects on the oxidation capacity and enhance surface ozone in the Arctic summer by a factor of 2–3 (Granier et al., 2006).

Similar to ozone, aircraft emissions have the largest effect on OH in the upper troposphere of the northern extratropics during summer. Despite the fact that the absolute perturbation is about a factor of 2 lower during winter, the relative perturbation exceeds 0.6% (or 12% scaled). The larger relative change during northern winter is due to the strong seasonal variation of the background latitudinal OH distribution. During winter the extratropical zonal mean OH at 300 hPa is less than $5{\cdot}10^3$ molecules/cm^3, whereas in summer the mean OH in the same region is reaching $1.3{\cdot}10^4$ molecules/cm^3.

Note that aircraft emissions have the maximum impact on OH over the subtropical Atlantic south of the main North Atlantic flight corridor. Larger humidity values and the smaller solar zenith angles at lower latitudes during that time of the year are more favourable for OH production than further north. Notice that ship emissions also significantly contribute to the OH perturbation in the middle to upper troposphere of the subtropics up to 200 hPa caused by convective uplift of NO_x from maritime transport in the tropical and subtropical latitudes.

5.2 Methane lifetime

As seen in the previous section ship emissions have the largest effect on OH leading to the largest reduction of methane lifetime (Table 7) among the three major modes of transport. Methane lifetimes were calculated offline using the monthly mean CH_4 and OH-fields from each model. Note that no feedback factor is applied here, which would account for long-term equlibration to the new steady-state value as described in Fuglestvedt et al. (1999).

Note further that our results are deduced from a small scale perturbation and that OH is unlikely to respond linearly to a NO_x perturbation. We report here on the scaled values since the radiative forcing calculations were performed using the full scale perturbations to allow a robust signal to be obtained (see below). Based on our results road emissions are only half as efficient in perturbing OH on a global scale, and the effects of air traffic are the smallest. The changes by 4.12% (ensemble mean) due to ship emissions exceed the 1.56% reported by Eyring et al. (2007), but are close to Fuglestvedt et al. (2008), who reported 5.2%. The NO_x emissions in

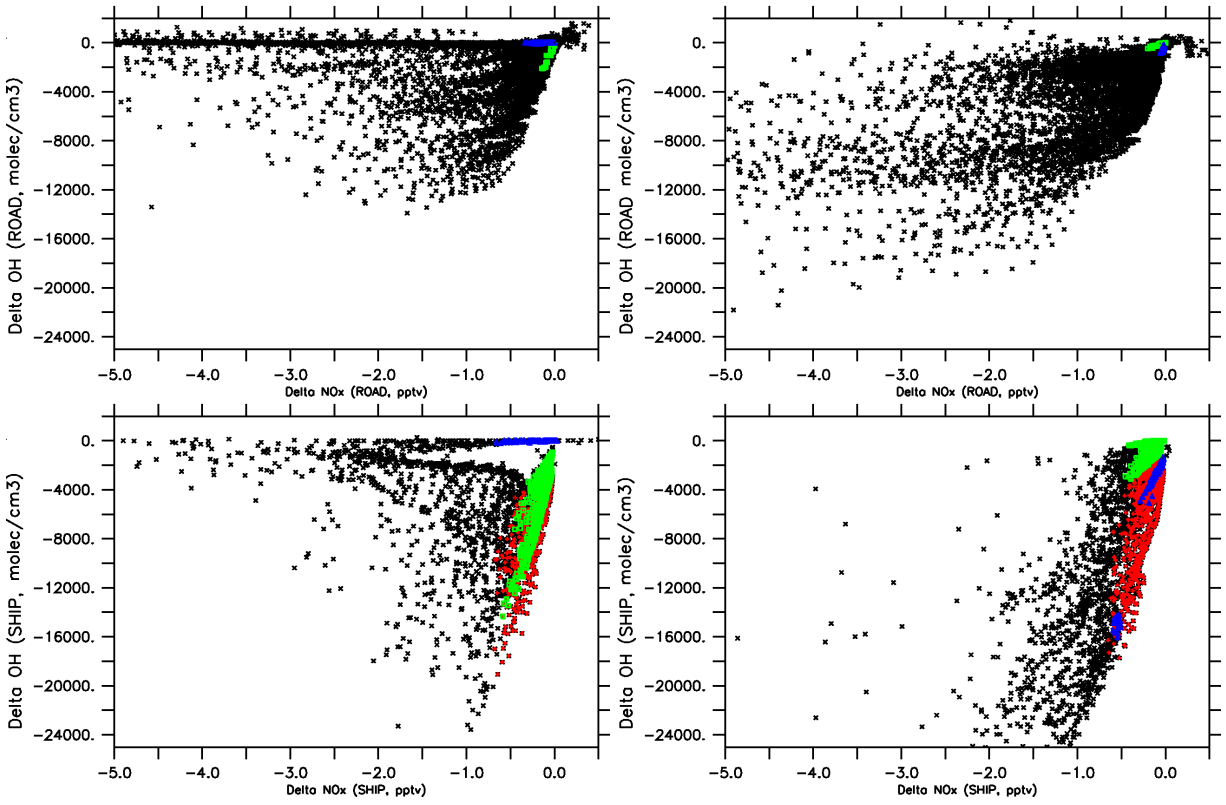

Fig. 11. Correlations between ΔOH and ΔNO_x for road traffic (upper row) and ship traffic (lower row) for January (left) and July (right). All coloured points are for low NO_x conditions coded by latitudes: (sub-)tropics (red), northern hemisphere (blue $>$ 30° N) and southern hemisphere (green, $<$ 30° S). The effect of ship emissions is shown at 950 hPa over the oceans and of road emissions over land up to 850 hPa.

Eyring et al. (2007) of 3.1 TgN/yr are lower compared to the 4.4 TgN/yr in this study (see Table 1) and also in Fuglestvedt et al. (2008), but it is unlikely that this alone has caused the large differences. In addition the emission patterns of both ship emission data sets are very different. The distribution of the ship emissions in Eyring et al. (2007) and Stevenson et al. (2006) is based on the EDGAR3.2 dataset, where the emissions are mainly concentrated on the major shipping routes. The ship emissions used in QUANTIFY have been generated by merging the daily fields of COADS and AMVER data (Automated Mutual-assistance Vessel Rescue system) (Endresen et al., 2003) and are distributed over a larger area (comp. Fig. 1 and Eyring et al. (2007), their Fig. 1). This explains the stronger effect on CH_4 lifetime, since a larger fraction of NO_x is emitted over the tropical oceans over a widespread area. Recall that conditions for OH production are favourable at low latitudes and in addition the local CH_4 lifetime by OH oxidation is shortest also due to the high temperatures.

Both factors are also the reason for the smaller effects of road and aircraft emissions on OH and on the methane lifetime, since they occur in higher latitudes and altitudes where annual mean OH concentrations and temperatures are lower.

5.3 Sensitivity of OH production

From Fig. 10 it is evident that ship emissions strongly affect the still relatively clean regions mostly in the tropics, but also in the extratropics. In contrast, road emissions are largely released into an environment already affected by emissions from other sources both of natural (soils, lightning) and anthropogenic origin. The different effects on OH from road and ship traffic in the boundary layer are presented in Fig. 11 showing the ΔNO_x and ΔOH perturbations for road and ship emissions, respectively. Coloured data points are indicative for low NO_x conditions ($<$ 20 pptv) in different latitude belts. The correlations show that the sensitivity of OH to NO_x perturbations is much higher for ship traffic than for road emissions even under low-NO_x conditions. As expected the ΔOH/Δ NO_x-ratio is highest for ship emissions in the relatively pristine maritime conditions in the tropics (red). The impact of road emissions is insignificant in these regions under low-NO_x conditions. In particular in the southern extratropics (green dots) there is a high sensitivity to NO_x perturbations from ships.

In relatively NO_x enriched conditions, under which most of the road emissions occur, the effect of ship NO_x on OH is also higher than that of road traffic. The OH response

Table 8. Radiative forcings from changes in ozone, changes in methane and methane-induced ozone change by model and transportation sector in mW/m^2. Note that the fully scaled perturbations were used to calculate the forcings

	ROAD				SHIP				AIRCRAFT			
	O_3	CH_4	$O_{3(CH_4)}$	total	O_3	CH_4	$O_{3(CH_4)}$	total	O_3	CH_4	$O_{3(CH_4)}$	total
TM4	26.3	−16.8	−7.0	2.5	23.8	−29.3	−12.3	−17.8	12.7	−7.3	−3.1	2.3
OSLO	32.7	−12.3	−5.1	15.3	30.0	−32.7	−13.7	−16.5	10.8	−5.7	−2.4	2.8
LMDz	32.8	−17.2	−7.2	8.4	26.1	−37.1	−15.6	−26.6	14.4	−9.6	−4.0	0.8
UCI	28.3	−11.5	−4.8	11.9	29.4	−31.6	−13.3	−15.6	13.2	−8.4	−3.5	1.3
TOMCAT	19.2	−14.7	−6.2	−1.7	27.24	−55.0	−23.1	−50.8	30.2	−16.1	−6.8	7.3
mean	27.9	−14.5	−6.1	7.3	27.3	−37.2	−15.6	−25.5	16.3	−9.4	−4.0	2.9
σ	5.0	2.3	1.0	6.2	2.2	9.3	3.9	13.3	7.1	3.6	1.5	2.3

for ship emissions is an almost linear function at the lower ΔNO_x levels, whereas the efficiency of OH production from road is weaker and levels off at lower ΔNO_x perturbations. OH perturbations from road NO_x emissions maximize at $2{\cdot}10^4$molecules/cm^3, while OH perturbations from ship exceed $2.5{\cdot}10^4$molecules/cm^3 and show no saturation tendency. This can be attributed to the higher level of NMHCs and NO_2 over the continents acting as a sink for OH at high pollution levels.

5.4 Radiative forcings

We briefly report the radiative forcings resulting from the transport-induced ozone changes using the mean perturbations scaled to 100% to obtain a robust signal. The ozone radiative forcing (cloudy skies including stratosphere temperature adjustment) was calculated using the University of Oslo radiative transfer code (e.g. Myhre et al., 2000). The forcing was calculated using the 3-D monthly mean ozone perturbation fields generated by each of the participating models. The annual and global-mean forcings are shown in Table 8. Averaged over the models, the road and shipping induced forcings are about the same (27 mWm^{-2}) with aviation contributing around 16 mWm^{-2}. However this hides significant intermodel differences. For three models, the road forcing is highest, followed by shipping followed by aviation. For p-TOMCAT this order of importance is reversed.

The forcings are within their stated uncertainties in broad agreement with those reported by Fuglestvedt et al. (2008) except for road traffic, for which a value of 54±11 mWm^{-2} was reported. A main reason for the weaker radiative forcing is the use of lower road emissions in this study compared to Fuglestvedt et al. (2008). Note further that we use a small perturbation approach. As shown in Sect. 2.1 the ozone response to a perturbation of road traffic emissions is smaller compared to a total decline of the road emission source. Thus, the ozone burden change and the associated radiative forcing are likely to be smaller.

Table 8 also shows simple estimates for two further forcings which result from the emissions and the consequent ozone and OH changes – the change in methane and the resulting change in ozone. These estimates are derived following the method given in Berntsen et al. (2005). First, the change in methane is calculated from the scaled percentage change in lifetime given in Table 7, multiplied by a feedback factor of 1.4 to account for the impact of methane changes on its own lifetime. The radiative forcing is then calculated assuming a methane specific forcing of 0.37 mWm^{-2} ppbv^{-1}, which is a linearization of the IPCC (2001) forcing for a background methane mixing ratio of 1740 ppbv and a nitrous oxide mixing ratio of 319 ppbv. Second, the radiative forcing due to the methane-induced ozone change (see Eq. B6 of Berntsen et al. (2005)) is estimated using multimodel means of both the response of ozone to a methane change (a 10% increase in methane leads to a 0.64 DU increase in ozone) and an ozone specific radiative forcing of 42 mWm^{-2} DU^{-1} from IPCC (2001). Together these lead to a methane-induced ozone radiative forcing which is 0.42 times the methane radiative forcing. This method assumes that the methane change is in equilibrium with the change in OH, which will require several decades of constant emissions to achieve.

The mean "net" forcing from the three components (Table 8) is positive for road and aviation and negative for shipping, as also found by Fuglestvedt et al. (2008). However, the residual nature of this net forcing leads to large intermodel differences, particularly for road and air where the standard deviation is almost as large as the mean. For aircraft emissions the effect on ozone and methane as calculated for the individual models is on average somewhat weaker as in Sausen et al. (2005), which can partly be attributed to the small perturbation approach, but also to the higher model resolution used here (Rogers et al., 2002).

All models simulate much stronger forcings for ship emissions compared to Eyring et al. (2007) which is most likely due to the very different distribution of the emissions, but also due to lower emission estimates of NO_x as stated in the previous section. Fuglestvedt et al. (2008) obtain forcings of 32±9 mWm^{-2} for ozone and −43±13 mWm^{-2} for methane, which both cover the range of our individual model

simulations. Similarly, our results indicate a strong effect of ship emissions on OH and therefore methane lifetime. Thus, the net effect on radiative forcing from ship emission induced ozone and methane lifetime changes is strongly negative.

For road and aircraft the ozone perturbations particularly in the upper troposphere as shown in Figs. 6–7, lead to a total positive forcing, compensating the methane forcing. This also indicates the importance of convection for the vertical transport of road emissions and ozone precursors, which is more efficient over land compared to convection over the ocean, where ship emissions occur.

6 Conclusions

In the frame of QUANTIFY the combined and relative effects of road, ship and aircraft emissions on the composition of the current atmosphere have been investigated. Six models simulated the effects of traffic on the current state of the atmosphere using a small (5%) perturbation approach. The results highlight the global impact of ship emissions on the chemical state of the marine boundary layer. Directly at the surface their impact can exceed 0.5% relative to the ozone backround contributing 60–80% to the total perturbation by traffic. They strongly contribute to the tropospheric ozone column perturbation of 0.2 DU over the Atlantic Ocean.

For the global OH budget the effect of ship emissions is most important. Based on the small 5% perturbation it accounts for an OH-perturbation up to $2.5{\cdot}10^4$ molecules/cm^3 equivalent to about 0.8% relative to the base case. Since emissions of NO_x largely occur in the pristine regions in the (sub-)tropics they efficiently lead to OH-formation and to additional ozone production. The consequent reduction of methane lifetime is about 0.2% for ship traffic, which is more than twice the value of road and aviation (0.9% and 0.5%, respectively).

Road emissions in the northern hemisphere affect ozone in particular during summer, when the low solar zenith angles in the extratropics enhance photochemistry. Continental convection leads to vertical redistribution of the road emissions resulting in a significant contribution to the ozone perturbation in the northern extratropical UTLS. Although air traffic has the strongest effect on upper tropospheric ozone mixing ratios between 30–60° N particularly road emissions have a substantial impact on ozone in that region also on the global scale.

The efficiency of ozone production per NO_x molecule emitted is highest for aircraft emissions being three times higher than the emissions from ships, which in turn perturb ozone more efficiently than NO_x from road traffic. The high efficiency of air traffic on ozone perturbations arises from the relatively long lifetime of NO_x and its reservoir species PAN and HNO_3 at the altitudes where the emissions occur.

Based on the fully scaled perturbations our results indicate the strongest mean positive sensitivities of road emissions on radiative forcing ($7.3{\pm}6.2\,\mathrm{mWm^{-2}}$) due to a strong response of ozone in the upper troposphere. Aircraft induced forcings on ozone and methane are somewhat lower (16.3 and $-9.4\,\mathrm{mWm^{-2}}$, respectively) also leading to a net positive forcing of $2.9{\pm}2.3\,\mathrm{mWm^{-2}}$. Ship emissions exert a negative forcing by $25.5{\pm}13.2\,\mathrm{mWm^{-2}}$ since they strongly affect OH and therefore the methane lifetime in the lower troposphere.

Acknowledgements. The QUANTIFY project is funded by the European Union within the 6th research framework programme under contract 003893.

The service charges for this open access publication have been covered by the Max Planck Society.
Edited by: K. Carslaw

References

Andreae, M. and Merlet, P.: Emission of trace gases and aerosols from biomass burning, Global Biogeochem. Cy., 15, 955–966, 2001.

Berntsen, T., Fuglestvedt, J., Joshi, M., Shine, K., Stuber, N., Ponater, M., Sausen, R., Hauglustaine, D., and Li, L.: Climate response to regional emissions of ozone precursors: sensitivities and warming potentials, Tellus B, 57B, 283–304, 2005.

Bian, H. and Prather, M.: Fast-J2: Accurate Simulation of stratospheric photolysis in global chemical models, J. Atmos. Sci., 41, 281–296, 2002.

Borken, J. and Steller, H.: Report on the Draft Emission Inventories for Road Transport in the year 2000, Tech. rep., Deutsches Institut für Luft- und Raumfahrt (DLR), Institut für Verkehrsforschung, 2006.

Borken, J., Steller, H., Meretei, T., and Vanhove, F.: Global and country inventory of road passenger and freight transportation – Their fuel consumption and their emissions of air pollutants in the year 2000, Transport. Res. Rec., 2011, doi:10.3141/2011-14, 2007.

Brasseur, G. P., Müller, J., and Garnier, C.: Atmospheric impact of NO_x emissions by subsonic aircraft: A three-dimensional model study, J. Geophys. Res., 101, 1423–1428, 1996.

Cariolle, D., Evans, M., Chipperfield, M., Butkovskaya, N., Kukui, A., and LeBras, G.: Impact of the new HNO_3-forming channel of the HO_2+OH reaction on tropospheric HNO_3, NO_x, HO_x, and ozone, Atmos. Chem. Phys., 8, 4061–4068, 2008, http://www.atmos-chem-phys.net/8/4061/2008/.

Carver, G. and Scott, P.: IMPACT: an implicit time integration scheme for chemical species and families, Ann. Geophys., 18, 337–346, 2000, http://www.ann-geophys.net/18/337/2000/.

Carver, G., Brown, P., and Wild, O.: The ASAD atmospheric chemistry integration package and chemical reaction database, Comput. Phys. Commun., 105, 197–215, 1997.

Corbett, J. and Koehler, H.: Updated emissions from ocean shipping, J. Geophys. Res., 108, 4650, doi:10.1029/2003JD003751, 2003.

Dalsoren, S. and Isaksen, I.: CTM study of changes in tropospheric hydroxyl distribution 1990–2001 and its impact on methane, Geophys. Res. Lett., 33, L23811, doi:10.1029/2006GL027295, 2006.

Dameris, M., Grewe, V., Ponater, M., Deckert, R., Eyring, V., Mager, F., Matthes, S., Schnadt, C., Stenke, A., Steil, B., Brühl, C., and Giorgetta, M.: Long-term changes and variability in a transient simulation with a chemistry-climate model employing realistic forcing, Atmos. Chem. Phys., 5, 2121–2145, 2005, http://www.atmos-chem-phys.net/5/2121/2005/.

Endresen, O., Sorgand, E., Sundet, J., Dalsoren, S., Isaksen, I., Berglen, T., and Gravir, G.: Emission from international sea transportation and environmental impact, J. Geophys. Res., 108, 4560, doi:10.1029/2002JD002898, 2003.

Endresen, O., Sorgard, E., Behrens, H., Brett, P., and Isaksen, I.: A historical reconstruction of ships' fuel consumption and emissions, J. Geophys. Res., 112, D12301, doi:10.1029/2006JD007630, 2007.

Eyers, C., Norman, P., Middel, J., Plohr, M., Michot, S., Atkinson, K., and Christou, R.: AERO2K Global Aviation Emissions Inventories for 2002 and 2025, Tech. Rep. 04/01113, QinetiQ, http://elib.dlr.de/1328, 2004.

Eyring, V., Köhler, H., J., v., and Lauer, A.: Emissions from international shipping: 1. The last 50 years, J. Geophys. Res., 110, D17305, doi:10.1029/2004JD005619, 2005.

Eyring, V., Stevenson, D., Lauer, A., Dentener, F., Butler, T., Collins, W., Ellingsen, K., Gauss, M., Hauglustaine, D., Isaksen, I., Lawrence, M., Richter, A., Rodriguez, J., Sanderson, M., Strahan, S., Sudo, K., Szopa, S., van Noije, T., and Wild, O.: Multi-model simulations of the impact of international shipping on atmospheric chemistry and climate in 2000 and 2030, Atmos. Chem. Phys., 7, 757-780, 2007, http://www.atmos-chem-phys.net/7/757/2007/.

Folberth, G., Hauglustaine, D., Ciais, P., and Lathière, J.: On the role of atmospheric chemistry in the global CO_2 budget, Geophys. Res. Lett., 32, L08801, doi:10.1029/2004GL021812, 2005.

Fuglestvedt, J., Berntsen, T., Isaksen, I., Mao, H., Liang, X., and Wang, W.: Climatic forcing of nitrogen oxides through changes in tropospheric ozone and methane: global 3D model studies, Atmos. Environ., 33, 961–977, 1999.

Fuglestvedt, J., Berntsen, T., Myhre, G., Rypdal, K., and Skeie, R.: Climatic forcing from the transport sectors, P. Natl. Acad. Sci. USA, 105, 454–458, 2008.

Ganzeveld, L., van Aardenne, J., Butler, T., Lawrence, M., Metzger, S., Stier, P., Zimmermann, P., and Lelieveld, J.: Technical Note: Anthropogenic and natural offline emissions and the online EMissions and dry DEPosition submodel EMDEP of the Modular Earth Submodel system (MESSy), Atmos. Chem. Phys. Discuss., 6, 5457–5483, 2006, http://www.atmos-chem-phys-discuss.net/6/5457/2006/.

Gauss, M., Isaksen, I., Wong, S., and Wang, W.-C.: Impact of H_2O emissions from cryoplanes and kerosene aircraft on the atmosphere, J. Geophys. Res., 108, 4304, doi:10.1029/2002JD002623, 2003.

Gauss, M., Isaksen, I., Lee, D., and Sovde, O.: Impact of aircraft NO_x emissions on the atmosphere – tradeoffs to reduce impact, Atmos. Chem. Phys., 6, 1529–1548, 2006, http://www.atmos-chem-phys.net/6/1529/2006/.

Giannakopoulos, C., Chipperfield, M., Law, K., and Pyle, J.: Validation and intercomparison of wet and dry deposition schemes using 210Pb in a global three-dimensional off-line chemical transport model, J. Geophys. Res., 104, 23 761–23 784, 1999.

Granier, C. and Brasseur, G.: The impact of road traffic on global tropospheric ozone, Geophys. Res. Lett., 30, 1086, doi:10.1029/2002GL015972, 2003.

Granier, C., Niemeier, U., Jungclaus, J., Emmons, L., Hess, P., Lamarque, J.-F., Walters, S., and Brasseur, G.: Ozone pollution from future ship traffic in the Arctic northern passages, Geophys. Res. Lett., 33, L13807, doi:10.1029/2006GL026180, 2006.

Grewe, V.: Technical note: A diagnostic for ozone contributions of various NO_x emissions in multi-decadal chemistry-climate model simulations, Atmos. Chem. Phys., 4, 327–342, 2004, http://www.atmos-chem-phys.net/4/327/2004/.

Grewe, V.: Impact of climate variability on tropospheric ozone, Sci. Tot. Env., 374, 167–181, 2007.

Grewe, V., Brunner, D., Dameris, M., Grenfell, J., Hein, R., Shindell, D., and Staehelin, J.: Origin and variability of upper tropospheric nitrogen oxides and ozone at northern mid-latitudes, Atmos. Environ., 35, 3421–3433, 2001.

Grewe, V., Dameris, M., Fichter, C., and Sausen, R.: Impact of aircraft NO_x emissions. Part I: Interactively coupled climate-chemistry simulations and sensitivities to climate-chemistry feedback, lightning and model resolution, Meteorol. Z., 11, 177–186, 2002.

Grewe, V., Stenke, A., Ponater, M., Sausen, R., Pitari, G., Iachetti, D., Rogers, H., Dessens, O., Pyle, J., Isaksen, I., Gulstad, L., Sovde, O., Marizy, C., and Pascuillo, E.: Climate impact of supersonic air traffic: an approach to optimize a potential future supersonic fleet - results from the EU-project SCENIC, Atmos. Chem. Phys., 7, 5129–5145, 2007, http://www.atmos-chem-phys.net/7/5129/2007/.

Hauglustaine, D., Hourdin, F., Walters, S., Jourdain, J., Filiberti, M.-A., Lamarque, J.-F., and Holland, E.: Interactive chemistry in the Laboratoire de Météorologie Dynamique general circulation model: Description and background tropospheric chemistry evaluation, J. Geophys. Res., 109, D04314, doi:10.1029/2003JD003957, 2004.

Hedegaard, G., Brandt, J., Christensen, J. H., Frohn, L. M., and Geels, C., Hansen, K. M., and Stendel, M.: Impacts of climate change on air pollution levels in the Northern Hemisphere with special focus on Europe and the Arctic, Atmos. Chem. Phys., 8, 3337–3367, 2008, http://www.atmos-chem-phys.net/8/3337/2008/.

Hidalgo, H. and Crutzen, P.: The tropospheric and stratospheric composition perturbed by NO_x emissions of high-altitude aircraft, J. Geophys. Res., 82, 5833–5866, 1977.

Holtslag, A. A. M. and Boville, B.: Local vesus nonlocal boundary-layer diffusion in a global climate model, J. Climate, 6, 1825–1842, 1993.

Houweling, S., Dentener, F., and Lelieveld, J.: The impact of nonmethane hydrocarbon compounds on tropospheric photochemistry, J. Geophys. Res., 103, 10 673–10 696, 1998.

Hsu, J., Prather, M., and Wild, O.: Diagnosing the stratosphere-to-troposphere flux of ozone in a chemistry transport model, J. Geophys. Res., 110, D19305, doi:10.1029/2005JD006045, 2005.

Hsu, J. e. a.: Are the TRACE-P measurements representative of the western Pacific during March 2001?, J. Geophys. Res., 109, D02314, doi:10.1029/2003JD004002, 2004.

IPCC: Climate Change 2001: The scientific basis, Cambridge, UK, Intergovernmental Panel on Climate Change, 2001.

Isaksen, I., Zerefos, C., Kourtidis, K., Meleti, C., Dalsoren, S., Sundet, J., Grini, A., Zanis, P., and Balis, D.: Tropospheric ozone changes at unpolluted and semipolluted regions induced by stratospheric ozone changes, J. Geophys. Res., 110, D02302, doi:10.1029/2004JD004618, 2005.

Jöckel, P., Tost, H., Pozzer, A., Brühl, C., Bucholz, J., Ganzeveld, L., Hoor, P., Kerkweg, A., Lawrence, M., Sander, R., Steil, B., Stiller, G., Tanharte, M., Taraborrelli, D., van Aardenne, J., and Lelieveld, J.: Evaluation of the atmospheric chemistry GCM ECHAM5/MESSy: Consistent simulation of ozone in the stratosphere and troposphere, Atmos. Chem. Phys., 6, 5067–5104, 2006,
http://www.atmos-chem-phys.net/6/5067/2006/.

Kahn Ribeiro, S., Kobayashi, S., Beuthe, M., Gasca, J., Greene, D., Lee, D., Muromachi, Y., Newton, P., Plotkin, S., Sperling, D., Wit, R., and Zhou, P.: Transport and its infrastructure, in: Climate Change 2007: Mitigation. Contribution of Working Group III to the Fourth Assessment Report of the Intergovernmental Panel on Climate Change, IPCC, edited by Metz, B., Davidson, O., Bosch, P., Dave, R., and Meyer, L., Cambridge University Press, Cambridge, United Kingdom and New York, NY, USA, 2007.

Kentarchos, A. and Roelofs, G.: Impact of aircraft NO_x emissions on tropospheric ozone calculated with a chemistry-general circulation model: Sensitivity to higher hydrocarbon chemistry, J. Geophys. Res., 107, 4175, doi:10.1029/2001JD0000828, 2002.

Kerkweg, A. and, S. R., Tost, H., and Jöckel, P.: Technical note: Implementation of prescribed (OFFLEM), calculated (ONLEM), and pseudo-emissions (TNUDGE) of chemical species in the Modular Earth Submodel System (MESSy), Atmos. Chem. Phys., 6, 3603–3609, 2006,
http://www.atmos-chem-phys.net/6/3603/2006/.

Law, K. and Nisbet, E.: Sensitivity of the methane growth rate to changes in methane emissions from natural gas and coal, J. Geophys. Res., 101, 14 387–14 397, 1996.

Law, K., Plantevin, P., Shallcross, D., Rogers, H., Pyle, J., Grouhel, C., Thouret, V., and Marenco, A.: Evaluation of modelled O_3 using MOZAIC data, J. Geophys. Res., 103, 25 721–25 737, 1998.

Law, K., Plantevin, P., Thouret, V., Marenco, A., Asman, W., Lawrence, M., Crutzen, P., Muler, J., Hauglustaine, D., and Kanakidou, M.: Comparison between global chemistry transport model results and Measurement of Ozone and Water Vapor by Airbus In-Service Aircraft (MOZAIC) data, J. Geophys. Res., 105, 1503–1525, 2000.

Lawrence, M. G. and Crutzen, P. J.: Influence of NO_x emission from ships on tropospheric photochemistry and climate, Nature, 402, 167–170, 1999.

Lelieveld, J., Peters, W., Dentener, F., and Krol, M.: Stability of tropospheric hydroxyl chemistry, J. Geophys. Res., 107, 4715, doi:10.1029/2002JD002272, 2002.

Lelieveld, J., Dentener, F., Peters, W., and Krol, M.: On the role of hydroxyl radicals in the self-cleansing capacity of the troposphere, Atmos. Chem. Phys., 4, 2337–2344, 2004,
http://www.atmos-chem-phys.net/4/2337/2004/.

Lemke, P., Ren, J., Alley, R., Allison, I., Carrasco, J., Flato, G., Fujii, Y., Kaser, G., Mote, P., Thomas, R., and T., Z.: Observations: Changes in Snow, Ice and Frozen Ground, in: Climate Change 2007: The Physical Science Basis. Contribution of Working Group I to the Fourth Assessment Report of the Intergovernmental Panel on Climate Change, IPCC, edited by: Solomon, S., Qin, D., Manning, M., Chen, Z., Marquis, M., Averyt, K., Tignor, M., and Miller, H., Cambridge University Press, Cambridge, United Kingdom and New York, NY, USA, 2007.

Matthes, S., Grewe, V., Sausen, R., and Roelofs, G.: Global impact of road traffic emissions on tropospheric ozone, Atmos. Chem. Phys., 7, 1707–1718, 2007,
http://www.atmos-chem-phys.net/7/1707/2007/.

Meijer, E., van Velthoven, P., Brunner, D., Huntrieser, H., and Kelder, H.: Improvement and evaluation for the parametrisation of nitrogen oxide production by lightning, Phys. Chem. Earth, 26(8), 557–583, 2001.

Meilinger, S., Kärcher, B., von Kuhlmann, R., and Peter, T.: On the impact of heterogenous chemistry on ozone in the tropopause region, Geophys. Res. Lett., 28, 515–518, 2001.

Meilinger, S., Kärcher, B., and Peter, T.: Microphysics and heterogeneous chemistry in aircraft plumes – high sensitivity on local meteorology and atmospheric composition, Atmos. Chem. Phys., 5, 533–545, 2005,
http://www.atmos-chem-phys.net/5/533/2005/.

Myhre, G., Karlsdottir, S., Isaksen, I., and Stordal, F.: Radiative forcing due to changes in tropospheric ozone in the period 1980 to 1996, J. Geophys. Res., 105, 28 935–28 942, 2000.

Niemeier, U., Granier, C., Kornblueh, L., Walters, S., and Brasseur, G.: Global impact of road traffic on atmospheric chemical composition and on ozone climate forcing, J. Geophys. Res., 111, D09301, doi:10.1029/2006JD006407, 2006.

O'Connor, F., Carver, G., Savage, N., Pyle, J., Methven, J., Arnold, S., Dewey, K., and Kent, J.: Comparison and visualisation of high-resolution transport modelling with aircraft measurements, Atmos. Sci. Lett., 6, 164–170, doi:10.1002/asl.111, 2005.

Ohara, T., Akimoto, H., Kurokawa, J., Horii, N., Yamaji, K., Yan, X., and Hayasaka, T.: An Asian emission inventory of anthropogenic emission sources for the period 1980–2020, Atmos. Chem. Phys., 7, 4419–4444, 2007,
http://www.atmos-chem-phys.net/7/4419/2007/.

Olivier, J., van Aardenne, J., Dentener, F., Ganzeveld, L., and Peters, J.: Recent trends in global greenhouse gas emissions: regional trends and spatial distribution of key sources, in: Non-CO_2 Greenhouse Gases (NCGG-4), Millpress, Rotterdam, 325–330, 2005.

Pickering, K. E., Wang, Y., Tao, W., Price, C., and Muller, J.-F.: Vertical distribution of lightning NO_x for use in regional and global chemical transport models, J. Geophys. Res., 109, 31 203–31 216, 1998.

Prather, M.: Numerical advection by conservation of second-order moments, J. Geophys. Res., 91, 6671–6681, 1986.

Price, C. and Rind, D.: A simple lightning parameterization for calculating global lightning distributions, J. Geophys. Res., 97, 9919–9933, 1992.

Rogers, H., Teyssedre, H., Pitari, G., Grewe, V., van Velthoven, P., and Sundet, J.: Model intercomparison of the transport of aircraft-like emissions from sub- and supersonic aircraft, Meteorol. Z., 151–159, 2002.

Sausen, R., Isaksen, I., Grewe, V., Schumann, U., Hauglustaine, D., Lee, D., Myhre, G., Köhler, M., Pitari, G., Strordal, F., and Zerefos, C.: Aviation radiative forcing in 2000: An update on IPCC(1999), Meteorol. Z., 555–561, 2005.

Savage, N., Law, K., Pyle, J., Richter, A., Nüss, H., and Burrows, J.: Using GOME NO_2 satellite data to examine regional differences in TOMCAT model performance, Atmos. Chem. Phys., 4, 1895–1912, 2004, http://www.atmos-chem-phys.net/4/1895/2004/.

Schumann, U.: The impact of nitrogen oxides emissions from aircraft upon the atmosphere at flight altitudes - results from the AERONOX project, Atmos. Environ., 31, 1723–1733, 1997.

Schumann, U. (Ed.): Air pollution research report 68, Pollution from aircraft emissions in the North Atlantic flight corridor (POLINAT 2), European Commission, L-2985 Luxembourg, ISBN 92-828-6197-X, 1998.

Schumann, U. and Huntrieser, H.: The global lightning-induced nitrogen oxides source, Atmos. Chem. Phys., 7, 3823–3907, 2007, http://www.atmos-chem-phys.net/7/3823/2007/.

Schumann, U., Schlager, H., Arnold, F., Ovarlez, J., Kelder, H., Hov, O., Hayman, G., Isaksen, I., Staehelin, J., and Whitefield, P.: Pollution from aircraft emissions in the North Atlantic flight corridor: Overview on the POLINAT projects, J. Geophys. Res., 105, 3605–3632, doi:10.1029/1999JD900941, 2000.

Sovde, O. A., Gauss, M., Isaksen, I. S. A., Pitari, G., and Marizy, C.: Aircraft pollution – a futuristic view, Atmos. Chem. Phys., 7, 3621–3632, 2007, http://www.atmos-chem-phys.net/7/3621/2007/.

Stevenson, D., Dentener, F., Schultz, M., Ellingsen, K., van Noije, T., Wild, O., Zeng, G., Amann, M., Atherton, C., Bell, N., Bergmann, D., Bey, I., Butler, T., Cofala, J., Collins, W., Derwent, R., Doherty, R., Drevet, J., Eskes, H., Fiore, A., Gauss, M., Hauglustaine, D., Horowitz, L., Isaksen, I., Krol, M., Lamarque, J.-F., Lawrence, M., Montanaro, V., Müller, J.-F., Pitari, G., Prather, M., Pyle, J., Rast, S., Rodriguez, J., Sanderson, M., Savage, N., Shindell, D., Strahan, S., Sudo, K., and Szopa, S.: Multimodel ensemble simulations of present-day and near-future tropospheric ozone, 111, D08301, doi:10.1029/2005JD006338, 2006.

Tiedtke, M.: A Comprehensive Mass Flux Scheme for Cumulus Parameterisation on Large Scale Models, Mon. Weather Rev., 117, 1779–1800, 1989.

Tost, H., Jöckel, P., Kerkweg, A., Sander, R., and Lelieveld, J.: Technical Note: A new comprehensive SCAVenging submodel for global atmospheric chemistry modelling, Atmos. Chem. Phys., 6, 565–574, 2006, http://www.atmos-chem-phys.net/6/565/2006/.

Tost, H., Jöckel, P., and Lelieveld, J.: Lightning and convection parameterisations - uncertainties in global modelling, Atmos. Chem. Phys., 7, 4553–4568, 2007, http://www.atmos-chem-phys.net/7/4553/2007/.

van Aardenne, J., Dentener, F., Olivier, J., Peters, J., and Ganzeveld, L.: The EDGAR3.2 Fast Track 2000 data set (32FT2000), www.mnp.nl/edgar/model/v32ft2000edgar/docv32ft2000, Joint Research Center, Institute for Environment and Sustainability (JRC-IES), Climate Change Unit, TP280, 21020 Ispra, Italy, 2005.

van Noije, T., Eskes, H., Dentener, F., Stevenson, D., Ellingsen, K., Schultz, M., and Wild, O.: Multi-model ensemble simulations of tropospheric NO_2 compared with GOME retrievals for the year 2000, Atmos. Chem. Phys., 6, 2943–2979, 2006a, http://www.atmos-chem-phys.net/6/2943/2006/.

van Noije, T., Segers, A., and van Velthoven, P.: Time series of the stratosphere-troposphere exchange of ozone simulated with reanalyzed and operational forecast data, J. Geophys. Res., 111, D03301, doi:10.1029/2005JD006081, 2006b.

von Kuhlmann, R., Lawrence, M. G., Crutzen, P., and Rasch, P.: A model for studies of tropospheric ozone and nonmethane hydrocarbons: Model description and ozone results, J. Geophys. Res., 108, 4294, doi:10.1029/2002JD002893, 2003a.

von Kuhlmann, R., Lawrence, M. G., Crutzen, P., and Rasch, P.: A model for studies of tropospheric ozone and nonmethane hydrocarbons: Model evaluation of ozone related species, J. Geophys. Res., 108, 4729, doi:10.1029/2002JD003348, 2003b.

Wild, O., Sundet, J., Prather, M., Isaksen, I., Akimoto, H., Browell, E., and Oltmans, S.: Chemical transport model ozone simulations for spring 2001 over the western Pacific: Comparisons with TRACE-P lidar, ozonesondes, and Total Ozone Mapping Spectrometer columns, J. Geophys. Res., 108(D21), 8826, doi:10.1029/2002JD003283, 2003.